Hypothalamic bile acid-TGR5 signaling protects from obesity

Ashley Castellanos-Jankiewicz, Omar Guzmán-Quevedo, Valérie Fénelon, Philippe Zizzari, Carmelo Quarta, Luigi Bellocchio, Anne Tailleux, Julie Charton, Daniela Fernandois, Marcus Henricsson, et al.

HAL Id: inserm-03257931
https://inserm.hal.science/inserm-03257931

Submitted on 11 Jun 2021

Hypothalamic bile acid-TGR5 signaling protects from obesity

Ashley Castellanos-Jankiewicz, Omar Guzmán-Quevedo, Valérie S Fénelon, Philippe Zizzari, Carmelo Quarta, Luigi Bellocchio, Anne Tailleux, Julie Charton, Daniela Fernandois, Marcus Henricsson, et al.

HAL Id: inserm-03709620
https://www.hal.inserm.fr/inserm-03709620

Submitted on 30 Jun 2022

Hypothalamic bile acid-TGR5 signaling protects from obesity

Ashley Castellanos-Jankiewicz[1#], Omar Guzmán-Quevedo[1,2,3#¤], Valérie S. Fénelon[1], Philippe Zizzari[1], Carmelo Quarta[1], Luigi Bellocchio[1], Anne Tailleux[4], Julie Charton[5], Daniela Fernandois[6], Marcus Henricsson[7], Catherine Piveteau[8], Vincent Simon[1], Camille Allard[1], Sandrine Quemener[4], Valentine Guinot[4], Nathalie Hennuyer[4], Alessia Perino[9], Alexia Duveau[1], Marlène Maitre[1], Thierry Leste-Lasserre[1], Samantha Clark[1], Nathalie Dupuy[1], Astrid Cannich[1], Delphine Gonzales[1], Benoit Deprez[5], Gilles Mithieux[10], David Dombrowicz[4], Fredrik Bäckhed[7,11,12], Vincent Prevot[6], Giovanni Marsicano[1], Bart Staels[4], Kristina Schoonjans[9], Daniela Cota[1*]

[1]University of Bordeaux, INSERM, Neurocentre Magendie, U1215, F-3300 Bordeaux, France; [2]Laboratory of Neuronutrition and Metabolic Disorders, Instituto Tecnológico Superior de Tacámbaro, 61650 Tacámbaro, Michoacán, Mexico; [3]Pós-Graduação em Neuropsiquiatria e Ciências do Comportamento, Universidade Federal de Pernambuco, 50732-970 Recife, Pernambuco, Brazil; [4]University of Lille, INSERM, CHU Lille, Institut Pasteur de Lille, U1011-EGID, F-59019 Lille, France; [5]University of Lille, INSERM, Institut Pasteur de Lille, U1177 - Drugs and Molecules for living Systems, EGID, F-59000 Lille, France; [6]University of Lille, INSERM, CHU Lille, Laboratory of Development and Plasticity of the Neuroendocrine Brain, Lille Neuroscience & Cognition, UMR-S1172, EGID, F-59000, Lille, France; [7]The Wallenberg Laboratory, Department of Molecular and Clinical Medicine, Institute of Medicine, Sahlgrenska Academy, University of Gothenburg, 413 45 Gothenburg, Sweden; [8]University of Lille, INSERM, Institut Pasteur de Lille, U1177 - Drugs and Molecules for living Systems, F-59000 Lille,

France;[9]Institute of Bioengineering, Faculty of Life Sciences, Ecole Polytechnique Fédérale de Lausanne, 1015 Lausanne, Switzerland; [10]INSERM U1213 Nutrition, Diabetes and the Brain, University of Lyon 1 Faculté de Médecine Lyon-Est, 69372 Lyon, France;[11]Novo Nordisk Foundation Center for Basic Metabolic Research, Faculty of Health Sciences, University of Copenhagen, 2200 N Copenhagen, Denmark;[12]Region Västra Götaland, Sahlgrenska University Hospital, Department of Clinical Physiology, Gothenburg, Sweden.

*Correspondence and Lead contact: <u>daniela.cota@inserm.fr</u>

[#] These authors contributed equally

[¤]Present address: Laboratory of Neuronutrition and Metabolic Disorders, Instituto Tecnológico Superior de Tacámbaro, 61650 Tacámbaro, Michoacán, Mexico.

Summary

Bile acids (BA) improve metabolism and exert anti-obesity effects through the activation of the Takeda G protein-coupled receptor 5 (TGR5) in peripheral tissues. TGR5 is also found in the brain hypothalamus, but whether hypothalamic BA signaling is implicated in body weight control and in obesity pathophysiology remains unknown. Here we show that hypothalamic BA content is reduced in diet-induced obese mice. Central administration of BA or a specific TGR5 agonist in these animals decreases body weight and fat mass by activating the sympathetic nervous system, thereby promoting negative energy balance. Conversely, genetic downregulation of hypothalamic TGR5 expression in the mediobasal hypothalamus favors the development of obesity and worsens established obesity by blunting sympathetic activity. Lastly, hypothalamic TGR5 signaling is required for the anti-obesity action of dietary BA supplementation.

Together, these findings identify hypothalamic TGR5 signaling as a key mediator of a top-down neural mechanism that counteracts diet-induced obesity.

Introduction

Bile acids (BA) are cholesterol-derived molecules produced by the liver that exert hormone-like metabolic effects by binding to the nuclear farnesoid X receptors (FXR) and to the membrane-bound Takeda G protein-coupled receptors 5 (TGR5, gene name *Gpbar1*), which are both expressed in peripheral organs (Kuipers et al., 2014; Perino et al., 2020). BA-dependent activation of hepatic FXR inhibits BA synthesis, regulates lipid and glucose metabolism and contributes to hepatic gluconeogenesis, among other effects (Kuipers et al., 2014; Perino et al., 2020). Whilst, BA activation of TGR5 in intestinal L-cells and pancreatic β-cells stimulates the release of glucagon-like peptide-1 (GLP-1) and insulin, respectively, thereby improving glucose homeostasis (Kumar et al., 2012; Thomas et al., 2009). In monocytes and macrophages, TGR5 activation inhibits pro-inflammatory responses in the adipose tissue of mice fed a high-fat diet (HFD) (Perino et al., 2014). Dietary supplementation of specific BA, such as cholic acid (CA) or chenodeoxycholic acid (CDCA), prevents weight gain and leads to significant weight loss in diet-induced obese (DIO) mice, mainly through an increase in thermogenesis and energy expenditure (Teodoro et al., 2014; Watanabe et al., 2006). Circulating BA levels also correlate with energy expenditure in healthy humans (Ockenga et al., 2012) and with changes in energy and substrate metabolism in obese subjects undergoing Roux-en-Y gastric bypass surgery (Patti et al., 2009; Simonen et al., 2012). Mechanistically, the activation of TGR5 by BA increases thermogenesis in mouse and human brown adipocytes by promoting intracellular thyroid hormone activation through type 2 iodothyronine deiodinase (D2) and by stimulating mitochondrial respiration (Broeders et al., 2015; Watanabe et al., 2006). Besides, TGR5 activation in white adipocytes

4

participates in the beiging process by increasing β-oxidation and improving mitochondrial function (Velazquez-Villegas et al., 2018).

While these findings suggest a role for peripheral BA-TGR5 signaling in counteracting DIO, neuronal circuits located in the mediobasal hypothalamus (MBH) are known to regulate energy expenditure, thermogenesis and food intake (Clapham, 2012; Dietrich and Horvath, 2013) and may therefore contribute to BA-mediated effects on energy balance. Several pieces of evidence support this possibility: i) BA are found in the brain, where their levels correlate with circulating ones (Higashi et al., 2017; Parry et al., 2010); ii) under acute cholestasis, BA rapidly accumulate in the hypothalamus (Doignon et al., 2011); iii) TGR5 is expressed in the brain of rodents (Doignon et al., 2011; Maruyama et al., 2006) and humans (Kawamata et al., 2003), and it is found in neurons, astrocytes and microglia (Keitel et al., 2010; McMillin et al., 2015; Zuo et al., 2019). Nevertheless, whether hypothalamic BA-TGR5 signaling is implicated in energy balance and obesity pathophysiology remains unknown.

By using both pharmacological and genetic approaches combined with metabolic phenotyping, we show that activation of central TGR5 signaling counteracts DIO, whereas genetic downregulation of hypothalamic TGR5 promotes it. These effects involve modulation of food intake and of energy expenditure through the sympathetic nervous system (SNS), revealing a long-range BA-dependent hypothalamic mechanism that contributes to weight regulation under DIO.

Results and Discussion

Central TGR5 agonism counteracts obesity

To determine whether DIO alters peripheral or brain BA levels, we quantified circulating and hypothalamic BA in chow lean and DIO mice during the post-prandial state (2h after re-exposure to food following a 24h fast). Total plasma levels were not significantly altered by obesity (Figure 1A and Tables S1 and S2), but total hypothalamic BA content was reduced in DIO mice as compared to lean controls (Figure 1B). Changes in specific BA species were further observed in both plasma and hypothalamus of obese mice (Figure 1A and 1B). In particular, significant decreases in deoxycholic acid (DCA), taurodeoxycholic acid (TDCA), and taurocholic acid (TCA), which all act as TGR5 agonists (Kawamata et al., 2003), were detected in the hypothalamus of DIO mice (Figure 1B). Hypothalamic and plasma levels of the potent TGR5 agonist DCA, but not TDCA or TCA, significantly correlated (Figure 1C). While unconjugated BA like DCA can diffuse (Higashi et al., 2017), conjugated BA may need to be actively transported into the brain (Mertens et al., 2017). BA transporters are expressed by brain endothelial cells (Mertens et al., 2017). We therefore evaluated changes in the hypothalamic mRNA expression of different BA transporters after 2h refeeding, as compared to 24h fasting. Food intake tended to increase the expression of all BA transporters, with a significant effect observed for the bile salt export pump (*Bsep*) in chow, but not DIO animals (Figure 1D). In parallel, food intake reduced hypothalamic *TGR5* expression in lean controls, but not in DIO mice (Figure 1D). Thus, DIO leads to a decrease in the hypothalamic content and possibly in the signaling activity of BA species that act as TGR5 agonists, particularly in response to changes in energy availability.

Next, we tested whether central pharmacological activation of TGR5 affects food intake and/or body weight in DIO. Mice were acutely treated with an intracerebroventricular (icv) injection of the synthetic TGR5-specific agonist 3-(2-Chlorophenyl)-N-(4-chlorophenyl)-N,5-dimethyl-4-isoxazolecarboxamide (CCDC) (Evans et al., 2009; Jensen et al., 2013). After confirming central CCDC availability and excluding possible leakage into the periphery (Table S3), we evaluated the effect of increasing icv doses of CCDC, which were administered just before the onset of the dark phase, in 24h-fasted DIO mice. Acute administration of CCDC (5μg dose) significantly reduced food intake over time, with a robust reduction in 24h food intake and body weight gain as compared to vehicle-treated animals (Figure 1E and 1F). Similar effects were observed after icv administration of a mix of BA (Figure 1G and 1H) acting as TGR5 agonists [Figure S1A and (Kawamata et al., 2003)] as well as after delivery of CCDC in the MBH (Figure S1B and S1C).

Based on these findings, we studied the impact of 4 weeks icv administration of the drug (5μg/day). A robust reduction in body weight (Figure 1I) and fat mass (Figure 1J) was observed in DIO mice, with no changes in lean mass (Figure 1K). Central CCDC administration also reduced food intake (Figure 1L and S1D) and improved insulin responsiveness (Figure 1M and S1E). Importantly, CCDC was undetectable in plasma (Table S3), thereby demonstrating its brain-restricted action. Feed efficiency, a measure of body mass change due to caloric intake, was also reduced by central CCDC treatment (Figure 1N), implying that mechanisms other than reduced food intake contribute to the observed anti-obesity action.

Chronic central TGR5 agonism recruits the sympathetic nervous system

To address whether changes in energy expenditure contribute to the observed CCDC-mediated weight loss (Figure 1I), we performed indirect calorimetry analysis in a new cohort of DIO mice before treatment-induced differences in body weight became significant. Mice receiving chronic icv CCDC had increased energy expenditure during the dark phase (Figure 2A and S2A). This was accompanied by a trend (p=0.06) towards a decreased respiratory exchange ratio (RER) (Figure 2B), suggesting preferential use of lipids as energy substrate, with no significant changes in locomotor activity (Figure 2C). The increase in energy expenditure and the reduction in RER were blunted in the same CCDC-treated animals at thermoneutrality, with again no effects on locomotion (Figure 2A, S2 A-C), suggesting that chronic central TGR5 activation could be increasing SNS activity. Of note, there was no difference in the meal size between the treatments groups (Figure S2D and S2E). Furthermore, mRNA expression of β1, 2 and 3 adrenoreceptors (*Adrb1, Adrb2, Adrb3*), which regulate thermogenesis and lipolysis (Blaszkiewicz and Townsend, 2016; Clapham, 2012) and *Dio2* (the gene expressing the deiodinase enzyme D2), were increased respectively in the epidydimal white adipose tissue (WAT) and brown adipose tissue (BAT) from CCDC-treated DIO mice at standard housing temperature (22°C, Figure 2D and 2E), but unchanged at thermoneutrality (30°C, Figure 2F and 2G).

Long-range brain-to-periphery mechanisms control hepatic BA production, at least under conditions in which high BA levels may become toxic for the organism (Doignon et al., 2011). To address whether the observed increase in energy expenditure might have been due to brain-to-periphery feedback loops affecting circulating BA, we evaluated

plasma BA profiles after 10 days and 4 weeks of continuous icv CCDC administration in DIO mice. No changes in plasma total or specific BA species were observed after 10 days (Figure S2F) or 4 weeks (data not shown) of icv CCDC administration, suggesting that top-down neuronal mechanisms must mediate the phenotypic changes observed. To this end, we studied whether the SNS contributes to CCDC-mediated effects, by performing chemical sympathectomy with 6-hydroxydopamine (6-OH-DOPA), which blunted the expression of the rate limiting enzyme for catecholamine synthesis tyrosine hydroxylase (TH) (Vaughan et al., 2014), by 77.5% in epidydimal WAT and 46.6% in BAT (Figure S2G). Peripheral sympathectomy blunted the previously described effects (see Figure 1I-L) of chronic icv CCDC treatment on body weight, body composition and food intake (Figure 2H-K), demonstrating that chronic central TGR5 agonism reduces adiposity by stimulating SNS activity in DIO mice.

TGR5 activity in the MBH protects from obesity

To uncover the role of hypothalamic TGR5 in obesity pathophysiology, we selectively deleted TGR5 in the MBH of *TGR5*$^{f/f}$ mice (Thomas et al., 2009) via stereotaxic injection of AAV-Cag-Cre-GFP viral particles or control viruses (AAV-Cag-GFP). An additional group of C57BL/6J mice receiving AAV-Cag-Cre-GFP was used to exclude potential Cre-mediated off-target effects. The viral strategy employed targeted neurons rather than astrocytes or microglia (Figure S3A), and led to Cre recombination (Figure S3B) and a ~50% reduction of *TGR5* mRNA expression specifically in the MBH, but not in other brain regions (Figure S3C), demonstrating the validity of the approach.

Notably, once exposed to HFD, $TGR5^{f/f}$-AAV-Cag-Cre-GFP mice gained more weight than $TGR5^{f/f}$-AAV-Cag-GFP or C57BL/6J-AAV-Cag-GFP controls (Figure 3A). $TGR5^{f/f}$-AAV-Cag-Cre-GFP mice also showed increased fat mass relative to control groups (Figure 3B), with no changes in lean mass (Figure 3C), modest hyperphagia (Figure 3D and S3D) and higher feed efficiency (Figure 3E). Strikingly, when AAV-mediated hypothalamic $TGR5$ knockdown was carried out in already DIO $TGR5^{f/f}$ mice, a further increase in body weight (Figure 3F), fat mass (with no changes in lean mass, Figure 3G and 3H), food intake (Figure 3I and S3E) and feed efficiency (Figure 3J) was observed. Hence, loss of hypothalamic $TGR5$ promotes the onset and worsening of DIO.

The increased feed efficiency observed in $TGR5^{f/f}$-AAV-Cag-Cre-GFP mice led us to hypothesize that hypothalamic TGR5 signaling may affect peripheral energy handling via changes in SNS-dependent thermogenesis. Accordingly, when HFD-fed $TGR5^{f/f}$-AAV-Cag-Cre-GFP and control mice were acutely exposed to a cold challenge (4°C for 4 hours), which activates the SNS (Clapham, 2012), $TGR5^{f/f}$-AAV-Cag-Cre-GFP mice displayed decreased protein expression of the thermogenic marker uncoupling protein 1 (UCP-1) in the BAT (Figure 3K), decreased SNS-dependent phosphorylation of the lipolysis marker hormone sensitive lipase (HSL) in the WAT (Figure 3L), and blunted mRNA levels of molecular markers of thermogenesis, fatty acid use and glucose clearance, such as $Adrb3$, HSL ($Lipe$), insulin receptor ($Insr$), solute carrier family 2 member 4 ($Slc2a4$) and peroxisome proliferator activated receptor alpha ($PPAR\alpha$) in this tissue (Figure 3M). Thus, reducing hypothalamic $TGR5$ expression hinders SNS activity, possibly favoring DIO. Accordingly, at thermoneutrality (30°C), the phenotype of $TGR5^{f/f}$-AAV-Cag-Cre-GFP exposed to HFD was undistinguishable from controls (Figure 3 N-R).

Characterization of hypothalamic cell types implicated in TGR5-mediated effects on energy balance

To uncover possible hypothalamic cell types implicated in the TGR5 action on body weight control, we characterized the molecular identity of TGR5-expressing hypothalamic cells. To this purpose, we used an endogenous *TGR5*-gene promoter-driven reporter mouse model that expresses hemagglutinin (HA) and tandem Tomato (Tdt), which is used as a surrogate marker for *TGR5* expression (Figure S3F). FACS-sorting of hypothalamic cells was followed by qPCR of markers of neuronal populations known to influence energy balance. TGR5-positive cells were found to express neuropeptides (neuropeptide Y, *Npy*; proopiomelanocortin, *Pomc*), transcription factors (steroidogenic factor 1, *SF1*), neurotransmitter transporters (vesicular GABA transporter, *VGAT*; vesicular glutamate transporter 2, *vGlut2*), enzymes (*Th*; glutamate decarboxylase 1, *GAD1* gene coding for GAD67, Glutamate decarboxylase 2, *GAD2* gene coding for GAD65), and hormone receptors (leptin receptor, *Lepr*) (Figure 3S). To corroborate these findings, we quantified *TGR5* mRNA levels in specific sub-populations of GABAergic (VGAT-positive) and glutamatergic (vGlut2-positive) hypothalamic neurons. To achieve this, we employed laser capture microdissection analysis of individual fluorescent cells obtained from *VGAT*-ires-Cre and *vGlut2*-ires-Cre mice, which were stereotaxically injected with a pAAV-hSyn-DIO-mCherry in the MBH (Figure S3G). Comparable *TGR5* mRNA levels were observed in both GABAergic and glutamatergic neurons (Figure S3H), suggesting that both neuronal populations may contribute to the phenotypes observed after AAV-based deletion of hypothalamic *TGR5*.

Accordingly, the viral-mediated model used to delete *TGR5* led to Cre-mediated recombination in ~36.7% of GABAergic and ~39.8% of glutamatergic neurons (Figure 3T).

To finally confirm that the metabolic effects observed *in vivo* stem from hypothalamic neurons rather than from non-neuronal cells expressing the receptor, we targeted the expression of TGR5 in MBH astrocytes by using an AAV-Cre-mCherry expressing the Cre recombinase under the control of the promoter for the astrocytic gene glial fibrillary acidic protein (GFAP). Although this approach led to specific Cre expression in *GFAP*-positive cells (Figure S4A), to genomic *TGR5* recombination (Figure S4B), and decreased hypothalamic *TGR5* mRNA levels (Figure S4C), no changes in body weight, body composition, food intake, or feed efficiency were observed in these animals (Figure S4 D-H).

Hypothalamic TGR5 signaling contributes to the anti-obesity action of BA supplementation

Dietary supplementation with CA, its synthetic derivatives or other BA acting as TGR5 agonists reduce weight gain in DIO mice by increasing thermogenesis and energy expenditure (Thomas et al., 2009; Watanabe et al., 2006; Zietak and Kozak, 2016). As dietary supplementation with CA results in a significant, supraphysiological increase in circulating BA levels in mice (Song et al., 2011; Watanabe et al., 2006), likely reaching the brain, we asked whether hypothalamic TGR5 signaling contributes to the therapeutic effects exerted by the systemic delivery of TGR5 agonists. To test this hypothesis,

TGR5^{f/f}-AAV-Cag-Cre-GFP mice and their *TGR5^{f/f}*-AAV-Cag-GFP controls were fed with a HFD, supplemented or not with 0.5% CA, as in (Watanabe et al., 2006). CA supplementation prevented body weight gain over time in the controls (Figure 4A) and reduced food intake (Figure S5A and S5B), body weight and fat mass as well as feed efficiency by the end of the study (Figure S5 C-E). The decreased food intake (Figure S5A and S5B) was not due to aversion, since a food preference test showed that when having the choice, mice would eat the HFD supplemented with CA rather than chow (Figure S5F). Knockdown of hypothalamic *TGR5* increased body weight, fat mass, food intake and feed efficiency in both HFD-fed and HFD-CA fed mice (Figure 4A and S5 A-E). For each GFP- and Cre-treated groups, we then calculated the CA-induced % change in these parameters relative to the corresponding HFD-fed control and observed that the degree of efficacy of CA supplementation in reducing body weight, fat mass and feed efficiency was strongly diminished in mice with hypothalamic *TGR5* knockdown (Figure 4B, 4C and 4E). Whilst, the CA-induced decrease of food intake was not significantly modified by the hypothalamic *TGR5* knockdown (Figure 4D). Thus, systemic administration of TGR5 agonists, here through dietary supplementation with CA, requires functional hypothalamic TGR5 to efficiently prevent weight gain.

Our work places hypothalamic TGR5 as a key regulator of food intake and of SNS-driven effects on body weight through adipose signaling, and offers a new foundation for understanding the mechanisms involved in the anti-obesity efficacy of pharmacological strategies that modulate the BA-TGR5 pathway. The neuroanatomical and molecular studies presented reveal that both glutamatergic and GABAergic neurons expressing

TGR5 may be involved, further demonstrating that MBH TGR5-positive cells express molecular markers of specific neuronal types implicated in energy balance regulation. Differently, although hypothalamic astrocytes play a role in obesity pathophysiology (García-Cáceres et al., 2019), TGR5 on this specific cell population is not involved in this context. Further studies will have to determine whether TGR5 may modulate inflammatory or immune responses in glia, as already demonstrated in peripheral immune cells (Perino et al., 2014). Our data reveal that hypothalamic TGR5 is protective against body fat accumulation under HFD conditions and that brain-selective activation of TGR5 effectively reduces food intake, while downregulation of the receptor causes hyperphagia. However, TGR5 expressed in the periphery can also contribute to the regulation of feeding. Indeed, supplementation of CA in HFD can still reduce food intake in mice with hypothalamic TGR5 knockdown. Accordingly, BA stimulate satiety through activation of TGR5 in the nodose ganglia neurons (Wu et al., 2020), whereas other studies have shown that BA-mediated metabolic effects involve a gut-to-brain axis (Liu et al., 2018).

We now provide evidence of a hypothalamic BA-TGR5 pathway that is relevant for top-down regulation of body weight under obesogenic conditions. This implies that bidirectional brain-periphery mechanisms are engaged by BA to control metabolic responses at multiple levels. Thus, we propose a shift in the current view of BA metabolic actions, which should now include a central perspective.

Limitations of Study

While our study showed a critical role for hypothalamic TGR5 as a protective mechanism against DIO, our neuroanatomical and molecular studies do not allow pinpointing the exact neuronal population(s) that drives the observed effects, albeit we provide for the first time information on candidate cell types possibly involved. More studies are needed to investigate the underlying neuronal circuitry engaged by TGR5 and its translatability to the human condition.

Acknowledgements

Author contributions

Declaration of interest

The authors declare no competing interests.

Figure legends

Figure 1. Acute and chronic central TGR5 agonism counteracts obesity.

(A-B) Plasma and hypothalamic levels of total and specific BA species in chow lean and DIO mice. BA quantification was carried out after 2h re-exposure to food following a 24h fast. n of mice: **(A)** 8-9/group; **(B)** 4-9/group.

(C) Correlation between plasma and hypothalamic DCA levels. n=17 mice.

(C) mRNA expression of BA transporters *OSTα*, *Ntcp* and *Bsep* and of *TGR5* in the hypothalamus of 24 fasted or 2h re-fed chow lean and DIO mice. n of mice: 5-6/group (chow); 7/group (DIO).

(E-H) Effect of an acute icv infusion of the selective TGR5 agonist CCDC (2.5 or 5μg) **(E-F)** or a BA mix (5μg) **(G-H)** on 24-h food intake (E and G) and body weight (BW) (F and H) in DIO mice. Animals were fasted for 24-h before icv treatment and subsequent exposure to food. n of mice: **(E-F)** 6-9/group; **(G-H)** 10-12/group.

(I-N) Effects of chronic icv infusion of CCDC (5μg/day) or its vehicle on daily BW **(I)**, body composition **(J-K)**, food intake **(L)**, blood glucose levels during an insulin tolerance test **(M)** and feed efficiency **(N)** in DIO mice. **(L)** was calculated from the start of the icv treatment; **(J-K)** were calculated from values obtained one day before the end of the study. n=6-7 mice/group; **(M)** insulin tolerance test carried out at the end of the chronic icv treatment. n=9-16 mice/group.

Data are mean ± SEM. A repeated measures two-way ANOVA (E, G, I, M) and a one-way ANOVA (F), were carried out, followed by a Fisher's LSD test. For (A, B, D, H, J-L,

N), unpaired t-tests or Mann-Whitney *U* test were carried out. In (C), Pearson's correlation was carried out. In (D), unpaired t-tests were performed using ΔCT values; data are fold change from respective fasted group. *p<0.05, **p<0.01, ***p<0.001. See also Figure S1 and Tables S1-S3.

Figure 2. Chronic central TGR5 agonism increases energy expenditure by engaging the sympathetic nervous system.

(A) Energy expenditure (kcal/h) at normal housing temperature (22°C) and at thermoneutrality (30°C) during chronic icv infusion of CCDC or its vehicle. DIO mice were placed in calorimetric cages 8 days after micro-osmotic pump implantation. Grey areas indicate the night period; data are shown per hour. n=6 mice/ group.

(B) Effect of chronic icv infusion of CCDC or its vehicle on respiratory exchange ratio (RER) of mice in (A) during the night and the day period at 22°C. n=6 mice/group.

(C) Effect of chronic icv infusion of CCDC or its vehicle on locomotor activity of mice in (A) during the night and the day period at 22°C. n=6 mice/group.

(D-G) mRNA expression of lipolysis and thermogenesis markers in the WAT and BAT from chronic CCDC- and vehicle- treated DIO mice at 22°C **(D-E)**, and 30°C **(F-G)**. For **(F-G)**, mice were killed after 6 days at 30°C. n of mice: **(D)** 5-7/group; **(E)** 6-7/group; **(F)** 10-12/group; **(G)** 10-12/group.

(H-K) Effects of chemical sympathectomy with 6-OH-DOPA, followed by chronic icv infusion of CCDC (5µg/day) or its vehicle on BW **(H)**, body composition **(I-J)** and food

intake **(K)** in DIO mice. 6-OH-DOPA was injected i.p. (80mg/kg) during 3 consecutive days and animals were allowed to recover 1 week before the chronic icv treatment. n=9 mice/group.

Data are means ± SEM. For (A, B, C, H), a repeated measures two-way ANOVA was conducted followed by a Fisher's LSD test. For (D-G), unpaired t-tests were performed using ΔCT values; data are fold change from the vehicle group. For (I-K), unpaired t-tests were used. $*p<0.05$, $**p<0.01$, $***p<0.001$; $\#p<0.05$ treatment effect. See also Figure S2 and Table S1.

Figure 3. Knockdown of *TGR5* in the MBH favors obesity.

(A-E) BW **(A)**, body composition **(B-C)**, food intake **(D)** and feed efficiency **(E)** following bilateral AAV-Cag-GFP control injection or AAV-Cag-Cre-GFP mediated knockdown of TGR5 in the MBH in *TGR5^f/f^* or C57BL/6J mice. Animals were on chow and then switched to a HFD (arrow). n=6-8 mice/group.

(F-J) BW **(F)**, body composition **(G-H)**, food intake **(I)** and feed efficiency **(J)** of already DIO *TGR5^f/f^* mice following bilateral AAV-Cag-GFP control injection or AAV-Cag-Cre-GFP mediated knockdown of TGR5 in the MBH. n=9-10 mice/group.

(K-M) Protein quantification of UCP-1 in the BAT (**K**) and of pHSL in the WAT (**L**) following 4h of cold exposure of HFD-fed *TGR5^f/f^* mice with (Cre) or without (GFP) MBH knockdown of TGR5. Representative blots per each tissue are depicted to the right of each histogram. mRNA expression of genes **(M)** related to thermogenesis, fatty acid use

and glucose clearance in the WAT of 4h cold-exposed HFD-fed $TGR5^{f/f}$ mice with or without MBH knockdown of TGR5. n=6-7 mice/group.

(N-R) BW **(N)**, body composition **(O-P)**, food intake **(Q)** and feed efficiency **(R)** in $TGR5^{f/f}$-AAV-Cag-Cre-GFP and control mice switched to HFD and maintained at thermoneutrality (30°C). n of mice: **(N-P)** 10/group in; **(Q-R)** 9-10/group.

(S) mRNA expression levels of different neuropeptides, receptors, enzymes and neurotransmitter markers in FACS-sorted cells expressing or not $TGR5$. n=4 mice.

(T) Representative images of combined fluorescent *in situ* hybridization with immunohistochemistry showing that some Cre-GFP positive cells in the MBH express GAD65 (GABAergic neurons; left) and vGlut2 (glutamatergic neurons; right). Inserts show magnification of cells that co-express GFP and GAD65 or vGlut2 (yellow arrowheads), cells that only express GFP (green arrowheads) and cells that only express GAD65 or vGlut2, respectively (red arrowheads). Cells' nuclei were stained with DAPI. 3V: 3rd ventricle. Scale bars= 100µm; 10µm for the inserts.

Data are means ± SEM. A repeated measures two-way ANOVA (A, F, N) and a one-way ANOVA (B-E) were used, followed by a Fisher's LSD test. In (G-L) and (O-R), unpaired t-tests were used. In (M), unpaired t-tests were performed using ΔCT values; data are fold change from the control group. For (S), no statistical analysis performed due to undetectable mRNA in some samples. Data are fold change from FACS-sorted cells expressing $TGR5$, except when it was not detectable. *p<0.05, **p<0.01. See also Figures S3, S4 and Table S1.

Figure 4. Hypothalamic TGR5 contributes to the anti-obesity action of dietary BA supplementation.

(**A**) BW of *TGR5^{f/f}* mice with (Cre) or without (GFP) hypothalamic knockdown of *TGR5* exposed to either a HFD (black and red lines in A) or to a HFD enriched with 0.5% cholic acid (CA, grey and orange lines in A). (**B-E**) Magnitude of the effect of CA supplementation on BW change (**B**), fat mass change (**C**), food intake (**D**) and feed efficiency (**E**) in *TGR5^{f/f}* mice with (Cre) or without (GFP) hypothalamic knockdown of *TGR5*. n=8-10 mice/group.

Data are means ± SEM. For (A), a repeated measures three-way ANOVA, and for (B-E), unpaired t-tests were used. In (B-E), for CA-supplemented GFP- and Cre-treated groups, data are expressed as % change relative to the corresponding HFD-fed control groups. $^{***}p<0.001$; $^{\#\#\#}p<0.001$ effect of TGR5 knockdown. See also Figure S5 and Table S1.

STAR Methods

RESOURCE AVAILABILITY

Lead Contact

Further information and requests for resources and reagents should be directed to and will be fulfilled by the Lead Contact, Daniela Cota (daniela.cota@inserm.fr). All main resources and reagents are listed in the Key Resources Table.

Materials Availability

AAV-Cag-GFP and AAV-Cag-Cre-GFP correspond to virus n°1 and n°4 from our lab stock, respectively, and are available upon request. The *TGR5-Tdt* reporter (B6-*Gpbar1^{tm1Ciphe}*) mice are available upon request (upon MTA signature).

Data and Code Availability

This study did not generate any unique datasets or code.

EXPERIMENTAL MODEL AND SUBJECT DETAILS

All procedures involving live animals were approved and carried out in accordance with the National and European Directives 2013/63/EU, the French Ministry of Agriculture and Fisheries and the Ethical Committee of the University of Bordeaux and of the University of Lille for Animal Experimentation (authorizations #3959, #13394, #13395 and APAFIS#2617-2015110517317420 v5). Maximal efforts were made to avoid or reduce any suffering as well as to reduce the number of animals used.

Animals

Male C57BL/6J (Janvier, France) and $TGR5^{f/f}$ ($Gpbar1^{tm1.1Auw}$) mice on a C57BL/6J background and generated as described in (Thomas et al., 2009) were used starting at 7-weeks-old (23g on average). In related studies we also used male $vGlut2$-ires-Cre ($Slc17a6^{tm2(cre)Lowl}$/J, JAX stock # 016963), $vGat$-ires-Cre (B6J.129S6(FVB)-$Slc32a1^{tm2(cre)Lowl}$/MwarJ, JAX stock # 028862) and $TGR5$-Tdt reporter (B6-$Gpbar1^{tm1Ciphe}$) mice. Reporter mice for TGR5 expression were generated by classical ES cell technology at Ciphe (Marseille-Luminy, France). Briefly an Hemagglutin (HA) Tag was inserted 3' in frame with the unique TGR5 exon after stop codon removal in order to generate a tagged TGR5 protein and a tandem Tomato (Tdt) Tag was inserted downstream an IRES sequence in order to use Tdt expression as a surrogate marker for $TGR5$ expression (Figure S3F). HA and TdT expression was detected by qPCR in colon and ileum from reporter but not from control mice (Figure S3F).

Animals were single housed in standard plastic rodent cages under a 12:12 h reversed light/dark cycle (lights on at 2:00 h) at 22 ± 2°C. Cages and enrichment (cellulose nestlets, wooden sticks and cardboard tunnels) were changed fortnightly. Mice received a standard chow diet (Standard Rodent Diet A03, SAFE, France; 3.236 kcal/g; 13.5% calories from lipids, 25.2% calories from proteins and 61.3% calories from carbohydrates) and water *ad libitum*, unless otherwise stated. For the diet-induced obesity model, mice were switched to a commercial high-fat diet (HFD) (D12492, Research Diets Inc., USA; 5.24 kcal/g; 20% calories from proteins, 20% calories from carbohydrates, 60% calories from lipids) one week after arriving to the housing facility

and were maintained on the diet for 12 weeks before the start of experiments until reaching 40g on average. A commercial HFD enriched with 0.5% cholic acid (D07033001, Research Diets Inc.; 5.22 kcal/g; 20% calories from proteins, 20% calories from carbohydrates, 60% calories from lipids) that was matched to the HFD was used for studies on BA supplementation.

All animals were used in scientific experiments for the first time. This includes no previous exposures to pharmacological substances. Number of animals used in each experiment is indicated in the figure legends and in the statistical Table S1. Mice were allocated to experimental groups taking care to have similar body weight and fat mass content per group before the start of the experiments.

Cell line

Human embryonic kidney (HEK) 293 cells (ATCC[R] CRL-1573) were cultured in Eagles's Minimum Essential Medium (MEM) supplemented with 10% of Fetal Calf Serum (FCS) and 1% antibiotics and incubated at 37°C and 5% of CO_2.

Cells were seeded in 150-mm dishes at a density of 7 x 10^6 cells/dish in MEM supplemented with 10% FCS and incubated at 37°C for 24h before transfection.

METHOD DETAILS

Body weight, food intake, feed efficiency

Body weight was recorded weekly from all mice throughout the studies and daily when a particular experimental procedure was carried out. Food intake was recorded when a

particular experimental procedure was carried out, and is indicated further below. Food intake data were not normalized to body weight, since this normalization is not necessary when body weight is matched across the groups (Kaiyala and Schwartz, 2011), as it was the case for all our studies.

The feed efficiency was calculated by dividing the body weight gain of a given time period into the total caloric intake during this same time. Animals that crumbled their food made it impossible to quantify their intake and were therefore excluded from the food intake and feed efficiency analyses.

Body composition

Body composition analysis was performed *in vivo* by nuclear echo magnetic resonance imaging whole-body composition analysis (EchoMRI™ 900; EchoMedical Systems, USA), as described previously (Cardinal et al., 2014). Analysis was performed at arrival to the housing facility, after the 12-week exposure to the HFD, and during chronic experiments, as indicated below. Briefly, mice were weighed and placed in the EchoMRI™ using a movement restrainer to allow proper measurements. All measures were taken in duplicates at the same time of day under free-feeding conditions. Data for fat and lean mass were extracted for analysis.

Surgeries

Mice were anesthetized using isofluorane 5% to induce the anesthesia and 1-2% during the surgery. Subcutaneous buprenorphine (0.1 mg/kg) and lidocaine at the level of the skull (0.1mL at 0.5%) were injected prior to surgery to reduce discomfort. Unconscious mice were placed on a stereotactic frame (David Kopf Instruments, USA); heat pads were used throughout the duration of the surgery to keep the body temperature stable. Eye ointment was applied to keep the eyes from drying. An incision was made to the skin to expose the skull after fur removal and asepsis with an iodine solution (Betadine®). For acute icv cannula placement, a burr hole for the stainless steel guide cannula (C313GS-5/SPC, G22; Plastics One®) was drilled on the skull (AP: -0.5; ML: -1.2; DV: -2.1). For chronic icv cannula placement, the same procedure as described above was used (AP: -0.3; ML: -1.0; DV: -2.5), with the addition of the subcutaneous implantation of a micro-osmotic pump (Alzet® System, model 1004; pump rate 0.1µl/h during 28 days), which were connected to the icv cannula through a catheter. For the acute intra-hypothalamic cannula placement, a bilateral stainless steel cannula (C235I-SPC, G33; Plastics One®) targeting the mediobasal hypothalamus was implanted (AP: -1.1; ML: ±0.4; DV: -4.9). All cannulae were fixed to the skull with stainless steel screws and dental cement (MajorRepair®). For bilateral viral injections, different viruses were used: AAV1/2-Cre-CAG-hrGFP (referred to here as AAV-Cag-Cre-GFP) or its control (AAV-Cag-GFP) (Hebert-Chatelain et al., 2016), ssAAV-2-hGFAP-mCherry_iCre-WPRE-hGHp(A) (identifier: v233; referred to here as AAV-GFAP-Cre-mCherry) or its control (identifier: v222; AAV-GFAP-mCherry), and pAAV-hSyn-DIO-mCherry (with a neuron-specific human synapsin promoter, Addgene, USA, #50459-AAV8). A craniotomy was made targeting the MBH (AP: -1.5; ML: ±0.3; DV: -5.8) and a 10 mm stainless steel injector (Nanofil® NF33BL, World Precision Instruments, USA) linked to a

10µL Hamilton syringe was slowly lowered into the target region to inject 500µL virus per side at 100nL/min. The injector was held in place for 3 min after injection to allow correct viral diffusion. Following surgery, all mice received 0.3 mL of saline solution subcutaneously, and meloxicam (5 mg/kg) for 2 days. Animals continued to be housed individually and body weight was monitored daily during one week to assess recovery.

Animal models

For acute icv experiments, a BA mix (sodium salts of taurocholic, glycocholic, deoxycholic, and cholic acids, Sigma-Aldrich) was diluted in artificial cerebrospinal fluid (aCSF), while 3-(2-chlorophenyl)-N-(4-chlorophenyl)-N, 5-dimethylisoxazole-4-carboxamide (Abcam), commonly known as CCDC, was diluted in 100% dimethylsulfoxide (DMSO) and delivered at the dose of 2.5 µg or 5 µg in a volume of 2 µL at a rate of 4 µL/min. Vehicles for the BA mix or CCDC consisted of 100% aCSF or DMSO, respectively. All acute drug infusions were carried out in 24 h fasted DIO C57BL/6J mice and compounds were administered just before the dark phase. Body weight was measured before and after 24 h from the icv administration; food intake was measured after 1, 2, 4 and 24 h from the icv administration. Correct cannula placement was assessed *in vivo* by icv infusion of neuropeptide Y (NPY; Phoenix Pharmaceuticals Inc.) in free-fed mice, as described previously (Bellocchio et al., 2013). Mice that ate >0.5g after 2 h of injection were included in the study.

For acute intra-hypothalamic experiments, DIO C57BL/6J mice bilaterally received CCDC (2 µg) or its vehicle at a volume of 0.2µL per side and a rate of 0.6µL/min. Body

weight and food intake were recorded as described above. Correct intra-hypothalamic cannula placement was confirmed by blue dye injection before killing and was used as a criterion for inclusion.

For chronic icv experiments, DIO C57BL/6J mice were implanted with micro-osmotic pumps that were filled with CCDC diluted in 60% DMSO and 40% aCSF (mean pumping rate: 0.09µL/h; mean fill volume: 91.9µL). The catheter linked to each pump was filled with enough volume of aCSF to allow 3 days of post-surgical recovery before the start of the CCDC infusion. The concentration of CCDC was calculated to allow the delivery of 5 µg CCDC over 24h (stock concentration of 2.33 µg/µL). A mix of 60% DMSO and 40% aCSF was used for vehicle-treated animals. Body weight and food intake were recorded daily for 4 weeks. Body composition was measured at the start, 1 week after micro-pump implantation and at the end of the chronic treatment. A separate group of mice receiving chronic CCDC treatment were placed in calorimetric cages at 22°C and then housed at thermoneutrality (30°C) during 6 days to evaluate energy expenditure under blunted sympathetic activity. Another group of mice underwent an insulin tolerance test after 4 weeks of chronic CCDC treatment. Details concerning these procedures are provided further below.

Chemical sympathectomy was carried out in DIO C57BL/6J mice by injecting i.p. for 3 consecutive days 80mg/kg of 6-hydroxydopamine (6-OH-DOPA) diluted in saline solution with 0.1% ascorbic acid (prepared fresh each day), as in (Quarta et al., 2010). One group of mice was killed after 1 week of the i.p. injections in order to assess the downregulation of tyrosine hydroxylase (TH) as marker of SNS activity in adipose tissues. After 1 week of 6-OH-DOPA administration, another group of mice underwent

stereotaxic surgery coupled with subcutaneous micro-pump implantation for chronic icv delivery of either vehicle or CCDC, as described earlier. Food intake and body weight were recorded daily for 4 weeks; body composition was measured at the start of the i.p. injections, 3 days after micro-pump implantation and at the end of the study.

For the targeted downregulation of TGR5 expression within the MBH, the AAV-Cag-Cre-GFP or its control were administered in the following *TGR5^{f/f}* models: lean mice on chow switched to a HFD and killed at 22°C (Cre linked AAV: $1.41E^9$ vg/mL; control: $1.17E^9$ vg/mL); lean mice on chow switched to a HFD and maintained at 30°C during HFD exposure (Cre linked AAV: $1.41E^9$ vg/mL; control: $1.17E^9$ vg/mL); lean mice on chow switched to a HFD for 2 weeks and killed after an acute cold challenge consisting of 4h exposure at 4°C (Cre linked AAV: $1.41E^{11}$ vg/mL; control: $1.17E^9$ vg/mL); DIO *TGR5^{f/f}* mice (Cre linked AAV: $1.41E^{11}$ vg/mL; control: $1.17E^9$ vg/mL); and lean *TGR5^{f/f}* mice on chow switched to a HFD or to a HFD enriched with 0.5% CA (Cre linked AAV: $1.41E^9$ vg/mL; control: $1.5E^{11}$ vg/mL). The AAV-GFAP-Cre-mCherry ($5.2E^{12}$ vg/mL) or its control ($6.0E^{12}$ vg/mL) were used for lean mice on chow switched to a HFD only. Viral localization within the MBH was assessed by neuroanatomical analysis. In all these models, food intake and body weight were recorded daily; body composition was measured at time of AAV injection and one day before killing.

For the targeted labelling of glutamatergic and GABAergic cells within the MBH, a pAAV-hSyn-DIO-mCherry ($2.1E^{13}$ vg/mL) was administered in chow-fed *vGlut2*-ires-Cre and *VGAT*-ires-Cre mice. Animals were killed after 3 weeks from the surgery for subsequent cell laser capture microdissection on the MBH (see further below).

Tissue collection

At the end of the *in vivo* experiments, mice were killed to obtain either fresh or perfused tissues, as mentioned per procedure.

For obtaining perfused brain tissue, mice were deeply anesthetized with an i.p. injection of sodium pentobarbital (300 µl/30g Exagon® mixed with 30 mg/kg lidocaine) and perfused transcardially with ice-cold phosphate buffer saline (PBS, pH 7.4), followed by 4% paraformaldehyde (PFA, Sigma-Aldrich, France). Whole brains were extracted and post-fixed in 4% PFA overnight at 4°C, then cryo-protected with a 30% sucrose solution in PBS at 4°C and frozen. Coronal sections (30µm) were cut with a cryostat (CM1950, Leica, Germany), collected, and stored in an antifreeze solution (30% ethylene glycol, 30% glycerol in KPBS) at -20°C until analysis.

For fresh tissue sampling, mice were killed by decapitation (for plasma collection) or dislocation, and tissues collected, frozen on isopentane chilled on dry ice, and stored at -80°C until needed for molecular and biochemical analysis.

Pharmacokinetics of CCDC

The abundance of CCDC was measured after an acute icv administration of 5µg, and after 4 weeks of continuous icv infusion. Groups of 3 mice were killed by decapitation at 15, 30, 60, 120 and 240 min after the acute icv injection, and the hypothalamus and the rest of the brain were collected as fresh tissue. Blood samples after acute or 4 weeks icv

CCDC administration were collected in heparin tubes, centrifuged at 5000 rpm for 10 min at 4°C, and plasma was collected and frozen at -80°C until analysis. Quantification was carried out by liquid-chromatography mass-spectrometry (LC-MS/MS).

Sample preparation

<u>Plasma:</u> Compound was extracted from plasma samples using a vortex, with an ice-cold acetonitrile/methanol (50:50) solution containing the internal standard, in a 1 to 10 ratio. After centrifugation (12000 rpm, 10 min, 4°C) of the homogenate samples, the supernatants were transferred into Matrix tubes for LC-MS/MS analysis.

The standard curve was generated using naïve mouse plasma (from vehicle animals), spiked with the appropriate compound solution resulting in 10 different concentrations of CCDC. This standard curve was then extracted as the plasma samples (in a 1 to 10 ratio) leading to concentration from 0.1 to 3000nM (0.1, 0.3, 1, 3, 10, 30, 100, 300, 1000 and 3000nM).

<u>Hypothalamus:</u> After 5 freeze-thaw cycles (4°C, 25min / -80°C, 25min), CCDC was extracted from hypothalamus in an acetonitrile/methanol (50:50) solution (9mL per gram of tissue) with 2 cycles of 10 minutes of sonication. After centrifugation (12000 rpm, 10 min, 4°C) of the homogenates, the supernatants were diluted in a 1 to 2 ratio with an ice-cold acetonitrile/methanol (50:50) solution containing the internal standard. Each tube was vigorously mixed, centrifuged (12000 rpm, 10 min, 4°C) then the supernatant was transferred into Matrix tubes for LC-MS/MS analysis.

Due to the small volume of hypothalamus homogenate available, the standard curve was generated using the appropriate CCDC solution (in acetonitrile/methanol), diluted in

a 1 to 2 ratio with an ice-cold acetonitrile/methanol (50:50) solution containing the internal standard, leading to concentration from 0.1 to 3000nM (0.1, 0.3, 1, 3, 10, 30, 100, 300, 1000 and 3000nM). Two points at 30 and 100nM final were prepared in the hypothalamus homogenate and no matrix effect was observed.

Rest of the brain: After 13 freeze-thaw cycles (4°C, 30min/-196°C, 5min), the rest of the brain was homogenate in a water/methanol (50:50) solution (1mL per gram of tissue) with 10 minutes of sonication. Then, after two more cycles of freeze-thaw (4°C, 30min / -196°C, 5min), the homogenates were extracted using an acetonitrile/methanol (50:50) solution (4mL per gram of tissue) with 2 cycles of 10 minutes of sonication. The samples were centrifuged (12000 rpm, 10 min, 4°C) then the supernatants were diluted in a 1 to 2 ratio with an ice-cold acetonitrile/methanol (50:50) solution containing the internal standard. Each tube was vigorously mixed, centrifuged (12000 rpm, 10 min, 4°C) and the supernatant transferred into Matrix tubes for LC-MS/MS analysis.

The standard curve was generated using naïve mouse brain (from vehicle animals), spiked with the appropriate compound solution resulting in 10 different concentrations of CCDC. This standard curve was then extracted as the brain samples (in a 1 to 2 ratio) leading to concentration from 0.1 to 3000nM (0.1, 0.3, 1, 3, 10, 30, 100, 300, 1000 and 3000nM).

LC-MS/MS

LC-MS/MS analysis was performed on an UPLC system Acquity I Class (Waters©), combined with a triple quadrupole mass spectrometer Xevo TQD (Waters©).

The column, placed at 40°C, was an Acquity BEH C18 50*2.1mm, 1.7µm column (Waters©) and the following mobile phases were used: 5mM ammonium formate pH 3.75 in water, as solvent (A) and 5 mM ammonium formate pH 3,75 in acetonitrile as solvent (B). At a flow rate of 600µL/min, the analytical method started at 98% (A) for 10s, then the percentage of B gradually increased at 98% until 2 min, hold at 98% (B) for 30s before returning to the initial conditions, hold 1.5 min. The samples were maintained at 10°C and the injection volume was 1µL.

MS analyses were performed under MRM detection using the following transitions: m/z 361.0 > 178.0 for CCDC with a cone voltage and a collision energy of 46 and 24V respectively; and 260.2 > 116.1 for the internal standard (propranolol, 100nM) with a cone voltage and a collision energy of 40 and 18V respectively. Argon was used as collision gas. The capillary voltage was set at 0.5 kV. The source temperature was 150°C, desolvation temperature was 600°C, desolvation gas flow was 1200 L.h-1 and cone gas flow was 50 L.h-1. All data were acquired and processed using the MassLynx 4.0 software (Waters©).

Insulin tolerance test

After 4 weeks of chronic icv infusion with CCDC or its vehicle, DIO mice were fasted for 6 h and were injected i.p. with 0.5 U/kg of insulin (Umuline Rapide, Lilly, France). Blood samples were collected from the tail vein and glucose was measured using glucose strips (OneTouch, Vita, France) at baseline, 15, 30, 60, 90 and 120 min after the administration of insulin.

Indirect calorimetry

Indirect calorimetry, in-cage locomotor activity and gas exchange analysis were carried out in light, temperature and humidity controlled calorimetric chambers (TSE Systems GmbH, Germany), as in (Cardinal et al., 2014). DIO mice receiving chronic icv infusion of CCDC or its vehicle were acclimated for 3 days in the chambers before recording. O_2 consumption and CO_2 production were measured every 20 min in order to calculate the gas exchange, the respiratory quotient and the energy expenditure. At the same time, in-cage locomotor activity was determined using a tridimensional infrared light beam system. Food intake was measured continuously by integration of scales inside the cages. A meal consisted of the consumption of at least 0.03g of food separated from the next feeding episode by at least 10 min (Hassouna et al., 2012). Body weight was measured daily during this time and the temperature was fixed to 22°C. When recording at thermoneutrality, the temperature in the calorimetric chambers was increased to 30°C.

Food preference test

Naïve *TGR5^{f/f}* lean mice were placed in individual cages and habituated to 2 food hoppers filled with chow and placed inside each cage for 5 days. During this time, mice were exposed to a small quantity of the HFD enriched with 0.5% CA to avoid neophobia during the behavioral experiment. On day 6, one food hopper was filled with the HFD supplemented with CA while the other continued to have chow. The hoppers with food

were removed from the cage 1 h before the preference test, which was performed during the light phase. Mice were then allowed access to the two hoppers during 1 h. The hoppers were weighed before and after access to food.

BA quantification

Depending on type of samples, the following BA species were quantified: CA, cholic acid; CDCA, chenodeoxycholic acid; DCA, deoxycholic acid; GCA, glycocholic acid; HDCA, hyodeoxycholic acid; LCA, lithocholic acid; TCA, taurocholic acid; TCDCA, taurochenodeoxycholic acid; TDCA, taurodeoxycholic acid; TLCA, taurolithocholic acid; TUDCA: tauro- ursodeoxycholic acid; TαMCA, tauro-α-muricholic acid; TβMCA, tauro-β-muricholic acid; TωMCA, tauro-ω-muricholic acid; UDCA, ursodeoxycholic acid; αMCA, α-muricholic acid; βMCA, β-muricholic acid; ωMCA, ω-muricholic acid.

BA quantification in chow-fed lean and DIO mice.

For plasma and hypothalamic BA measurements, chow lean and DIO mice were killed by decapitation 2 hours after re-exposure to either chow or HFD following a 24h fast. Plasma was obtained as described above in pharmacokinetics of CCDC. The hypothalamus was collected and immediately frozen in isopentane chilled on dry ice. Samples were stored at -80°C until analysis. BA were analyzed using ultra-performance liquid chromatography-tandem mass spectrometry (UPLCMS/MS) according to previous work (Tremaroli et al, 2015). Briefly, hypothalamic samples (15-20 mg wet weight) were homogenized and extracted in 500 μL of methanol containing deuterated internal standards (d4-TCA, d4-GCA, d4-GCDCA, d4-GUDCA, d4-GLCA, d4-UDCA, d4-CDCA,

d4-LCA; 25 nM of each). After 10 min of homogenization/extraction using the TissueLyser II instrument (Qiagen, Sweden) and 10 min of centrifugation at 20 000 g, the supernatant was evaporated under a stream of nitrogen and reconstituted in 100 μL methanol:water [1:1]. The samples were injected (5 μL) and BA were separated on a Kinetex C18 column (1.7 μ, 2.1 x 100 mm; Phenomenex, USA) using water with 7.5 mM ammonium acetate and 0.019% formic acid (mobile phase A) and acetonitrile with 0.1% formic acid (mobile phase B). The chromatographic separation started with 1 minute isocratic separation at 20% B. The B-phase was then increased to 35% during 4 min. During the next 10 min the B-phase was increased to 100%. The B-phase was held at 100% for 3.5 min before returning to 20%. The total runtime was 20 min. BA were detected using multiple reaction monitoring (MRM) in negative mode on a QTRAP 5500 mass spectrometer (AB Sciex, Canada) and quantification was made using external standard curves.

Plasma BA quantification in pharmacological studies

For measurements of circulating BA from chronic pharmacological studies, free-fed diet-induced obese mice were killed by decapitation after 10 days of chronic CCDC treatment. Briefly, plasma samples were thawed on ice, cold methanol was added for protein precipitation and samples were then vortexed 3 x 10 s and maintained at -20°C for 20 min. After centrifugation at 10,000 *g* for 10 min at 4°C, supernatants were transferred to clean tubes and dried in a speedvac concentrator, as done in (Garcia-Canaveras et al., 2012). The pellets were then reconstituted in methanol. The separation of BA was carried out on a Symmetry C18 Luna column (250 mm × 2.1 mm, particle size 5 μm) from Phenomenex (Le Pecq, France). The oven temperature was set

at 30°C. Solvent A was water containing 20 mM ammonium acetate, adjusted to pH 8 and solvent B was acetonitrile. Solvents were delivered at a total flow rate of 500 μl/min^{-1}. After a 5 min plateau with 28% B, the gradient profile was from 28% B to 90% B linearly in 15 min, followed by a 2 min plateau with 90% B. Column re-equilibration was performed for 4 min. The injection cycle was 26 min. BA quantification was then performed by high-performance liquid chromatography (UFLC-XR device; Shimadzu, Japan) coupled to tandem mass spectrometry MS/MS (QTRAP 5500 hybrid system, equipped with a Turbo VTM ion source; AB Sciex). Instrument control, data acquisition and processing were performed using the associated Analyst 1.5.2 software (AB Sciex). The inter- and intra-day precisions of the BA concentration assay are <15%, except for HCA and LCA (<30%).

Single cells laser capture microdissection

Four *vGlut2*-ires-Cre mice and 3 *VGAT*-ires-Cre mice having received a pAAV-hSyn-DIO-mCherry in the MBH were used. Coronal sections of perfused brains (10 μm thickness) covering the region from -1.34 to -1.94 mm caudal to bregma, as defined by Paxinos and Franklin, were made using a CM3050 S cryostat (Leica, Germany) and mounted on polyethyl-ene-naphthalate membrane 1mm glass slides (P.A.L.M. Microlaser Technologies AG, Germany) that were pretreated to inactivate RNase. Subsequently, sections were dehydrated in a series of pre-cooled ethanol baths (40s in 95% and twice 40s in 100%) and air-dried. Laser microdissection of mCherry-expressing cells was performed using a PALM MicroBeam microdissection system version 4.6

equipped with the P.A.L.M. RoboSoftware (P.A.L.M. Microlaser Technologies AG, Germany). Laser power and duration were adjusted to optimize capture efficiency. Microdissection was performed at 63X magnification. A total between 800/900 cells per mice was captured. Cells were collected in adhesive caps and re-suspended in PK buffer (PK buffer from RNeasy FFPE Kit, Qiagen), and stored at −80°C until extraction was done. Total RNA was extracted from microdissected cells using the RNeasy® FFPE Kit (Qiagen) according to the manufacturer's protocol. The integrity of the RNA was checked by capillary electrophoresis using the RNA 6000 Pico Labchip kit and the Bioanalyser 2100 (Agilent Technologies, France), and quantity was estimated by spectrophotometry using a Denovix DS-11 (Denovix, USA).

FACS of hypothalamic TGR5-expressing cells

The hypothalamus of 4 *TGR5-Tdt* reporter mice was microdissected and enzymatically dissociated using a Papain Dissociation System (Worthington, USA) to obtain a single-cell suspension. FACS (fluorescence-activated cell sorting) was performed using an ARIA SORP cell sorter cytometer device (BD Bioscience, Inc). The sorting parameter were based on measurements of Tomato fluorescence (excitation 561nm; detection: bandpass 675+/-20nm) by comparing cell suspensions from *TGR5-Tdt* and control animals. For each animal, 40 to 110 tomato-positive and an equal amount of tomato-negative cells were sorted directly into 10 µl of lysis buffer (0.1% Triton® X-100 and 0.4unit/µl RNaseOUT™, Life Technologies).

Quantitative Real-Time PCR (qPCR)

qPCR on tissues

qPCR was carried out in hypothalamic samples (reference genes: *Sdha* and *Tuba4a*) from chow-fed, lean and HFD-fed, DIO C57BL/6J mice, either fasted for 24h or re-exposed to food for 2h after the 24h fast. qPCR was also performed in epididymal white adipose tissue (WAT; reference genes: *Gapdh* and *Ppia*) and brown adipose tissue (BAT; reference genes: *Sdha* and *Nono*) from free-fed DIO mice receiving chronic CCDC treatment or vehicle killed by decapitation at 22°C; WAT and BAT from free-fed diet-induced obese mice receiving chronic CCDC treatment or vehicle and killed by decapitation at 30°C (reference genes: *Ppia* and *Nono*); WAT (reference genes: *Sdha* and *Nono*) from free-fed *TGR5^{f/f}* mice on a HFD that received AAV-Cag-Cre-GFP or its control and were killed by decapitation at 4°C; hypothalamus (reference genes *Ppia* and *Rpl13a*) from free-fed *TGR5^{f/f}* mice on a HFD that received the AAV-Cag-Cre-GFP or its control and were killed by perfusion at 22°C; and hypothalamus (reference genes: *Sdha*, *Eef1a1* and *Ywhaz*) from free-fed *TGR5^{f/f}* mice on a HFD that received the AAV-GFAP-Cre-mCherry or its control and were killed by perfusion at 22°C.

For samples from hypothalamic *TGR5* deletion models, 10 punches of 2 mm (cut from the 30 µm slices) containing the MBH, as well as the cortex, amygdala and ventral tegmental area (VTA), were obtained per animal, placed on 100µL proteinase K digest buffer (Qiagen) and frozen at 80°C until qPCR analysis.

Samples were homogenized in Tri-reagent (Euromedex, France). RNA from fresh tissue was isolated using a standard chloroform/isopropanol protocol, while RNA from perfused

samples was isolated using Quick-RNA^{TM} FFPE Kit (ZYMO Research). cDNA was synthesized from 2 µg of total RNA using Maxima Reverse Transcriptase (Fisher Scientific) and primed with oligo-dT primers (Fisher Scientific) and random primers (Fisher Scientific). qPCR was performed using a LightCycler® 480 Real-Time PCR System (Roche, France). qPCR reactions were done in duplicate for each sample (except on hypothalamic samples from mice receiving the AAV-GFAP-Cre-mCherry or its control, which were run in triplicates), using transcript-specific primers, cDNA (4 ng) and LightCycler 480 SYBR Green I Master (Roche) in a final volume of 10 µL. Primer sequences are reported in Table S4. Relative expression analysis was normalized against two reference genes (except on hypothalamic samples from mice receiving the AAV-GFAP-Cre-mCherry or its control, which were normalized to three reference genes), depending on the tissue (see above). The relative level of expression was calculated using the comparative $2^{-\Delta\Delta CT}$ method. mRNA expression levels are expressed as the fold change from the reference group (as mentioned in the figure legends) after normalization.

mRNA from colon and ileum samples of *TGR5-Tdt* reporter and control mice were extracted after shredding tissues in Trizol, phenol-chloroform extraction and precipitation by isopropanol was used. qPCR was performed to assess expression of *TGR5*, *HA*-tag and *Tandem Tomato*. *Ppia* was used as reference gene. Primer sequences are reported in Table S4.

qPCR on laser capture microdissected cells

cDNA was generated using the qScript XLT cDNA SuperMix (Quanta Biosciences) following the manufacturer's instructions. qPCR was performed as described above. Primer sequences are reported in Table S4. *Gapdh* and *Eef1a1* were used as reference genes.

qPCR on FACS-sorted cells

Total RNA obtained from FACS-sorted tomato-positive and -negative cells was reverse transcribed using high-capacity cDNA Reverse transcription kit (Applied Biosystems, # 4368814) after a DNAse treatment (DNase I, Amplification Grade, Invitrogen, #18068015). A linear preamplification step was performed using the TaqMan® PreAmp Master Mix Kit protocol (Applied Biosystems, # 4488593). Next, a real-time PCR was carried out on Applied Biosystems 7900HT Fast Real-Time PCR System using the TaqMan® probes (see Table S4) and TaqMan™ Universal Master Mix II (Applied Biosystems, # 4440049). Control housekeeping genes r18S and actin were used for analysis. Gene expression data were analyzed using the $2^{-\Delta\Delta Ct}$ method between negative and positive tomato FACS-sorted cells.

Western blot analysis

WAT and BAT samples from free-fed sympathectomized mice, as well as from free-fed TGR5$^{f/f}$ mice receiving the AAV-Cag-Cre-GFP or its control and sacrificed at 4°C were obtained after killing by decapitation.

Samples were homogenized in radioimmunoprecipitation assay buffer with phosphatase and protease inhibitors (Santa Cruz Biotechnology) for obtaining protein extracts. Proteins were separated in an SDS-polyacrylamide gel (9-13%) by electrophoresis and transferred to nitrocellulose membranes, which were then blocked for 1h with 5% skim milk powder and incubated overnight at 4°C with the following primary antibodies: hormone-sensitive lipase (HSL, 1:1000, #4107, Cell Signaling), phospho-HSL ser563 (1:1000, #4139, Cell Signaling), uncoupling protein-1 (UCP-1, 1:1000, #10983, Abcam), tyrosine hydroxylase (TH, 1:1000, #152, Millipore), and β-actin (1:2000, #4967, Cell Signaling), which was used as loading control. After washing in Tris-buffered saline with 0.05% Tween (TBST), the membranes were incubated for 1 h at room temperature with secondary antibody conjugated with horseradish peroxidase (goat anti-rabbit; 1:2000; Cell Signaling Technology). After 3 washes in TBST, immunoreactive bands were visualized using enhanced chemiluminescence (ECL Plus, PerkinElmer) then exposed on a ChemiDoc® MP Imaging System (Biorad). Bands were quantified using ImageJ software (NIH, USA). When necessary, membranes were stripped after protein detection for 10 min at 55°C with a solution containing 62.5 mmol/l Tris-HCl, 100 mmol/l 2-mercaptoethanol, and 2% SDS, blocked, and reblotted with another primary antibody.

Assessment of Cre recombination by PCR

Perfused brain slices containing the MBH from *TGR5^{f/f}* receiving the AAV-Cag-Cre-GFP or its control, or the AAV-GFAP-Cre-mCherry or its control were genotyped by PCR to evaluate recombination in genomic DNA. Tissue from naïve C57BL/6J mice (wild type,

WT) was used as a negative control, whilst tissues from whole body *TGR5* knockout obtained by crossing *TGR5*^*f/f* with *CMV*-Cre mouse strain (Schwenk et al., 1995) (referred as +/ex) was used as a positive control of excision. Five perfused brain slices per animal were incubated overnight at 56°C in Proteinase K buffer (100 mM Tris-HCl pH8, 5 mM EDTA, 0.2 % SDS, 200 mM NaCl, 0,2 mg/mL PK); after 10 min at 13200 rpm, the supernatants were purified by vacuum on silica columns, according to the manufacturer's protocol (Macherey-Nagel kit), on a Zephyr automatic workstation (Perkin-Elmer). PCR assay was carried out on a Bio-Rad C1000 thermal cycler, in a 20 μL volume, using GoTaq G2 Hot Start Green Master Mix (Promega), and 0.2 μM of each primer. PCR products were analyzed on a Labchip GX microfluidic electrophoresis system (Perkin-Elmer) using the DNA5k kit.

Neuroanatomical analysis

Perfused brain slices from *TGR5*^*f/f* mice receiving the AAV-Cag-Cre-GFP or its control, or the AAV-GFAP-Cre-mCherry or its control were analyzed.

Immunohistochemistry (IHC)

All immunofluorescence steps were performed under gentle agitation at room temperature. Slices were rinsed three times in PBS for 10 min and then incubated with primary antiserum overnight. Primary antibodies were diluted in PBS containing 0.3% Triton X-100 (PBST) and 5% normal serum (goat or donkey depending on the specie used to generate the secondary antibodies) except when Mouse on Mouse Fluorescein kit was used. After incubation, slices were washed again three times in PBS for 10 min

and incubated in secondary antibody solution for 2 h in the dark. Secondary antibodies were diluted in PBS containing 0.3% Triton X-100 except when Mouse on Mouse Fluorescein kit was used. After a 5 min rinse in PBS, slices were incubated 5 min with the nuclear marker 4',6'-diamidino-2-phenylindol (DAPI; 1:10000; # D1306, Molecular Probes). After a final rinse in PBS, slices were mounted on gelatin coated slides and coverslipped using Prolong gold anti-fade (# P36930, Vector Laboratories) and then stored at 4°C until use.

For visualization of microglia and neurons, we used a double immunohistofluorescent technique. Slices were incubated in a chicken antiserum against NeuN (1:500, #ABN91, Millipore) and in a rabbit antiserum against Iba-1 (1:2000, #019-19741, Wako). Slices were then incubated in a donkey anti-chicken secondary antibody conjugated to Alexa 647 (#703-606-155, Jackson ImmunoResearch Labs) and in a donkey anti-rabbit secondary antibody conjugated to Alexa 448 (#711-545-152, Jackson ImmunoResearch Labs) or to Alexa 594 (#711-585-152, Jackson ImmunoResearch Labs) for $TGR5^{f/f}$-AAV-GFAP-Cre-mCherry/$TGR5^{f/f}$-AAV-GFAP-mCherry and $TGR5^{f/f}$-AAV-Cag-Cre-GFP/$TGR5^{f/f}$-AAV-Cag-GFP mice respectively, all diluted 1:2000.

For visualization of astrocytes, we used a double immunohistofluorescent technique. We used a rabbit antiserum against GFAP (1:1000, #Z0334, Agilent) and a monoclonal mouse antibody against protein S100β-subunit (S100β, 1:10000, clone SH-B1, #S2532, Sigma-Aldrich). Slices obtained from $TGR5^{f/f}$-AAV-Cag-Cre-GFP/TGR5$^{f/f}$-AAV-Cag-GFP mice, after the initial PBS rinses, were incubated 30 min in 3%H_2O_2 PBST and rinsed three times in PBS for 5 min. After incubation in the primary antibodies, species-specific secondary antibodies which have been raised in goat [anti-rabbit conjugated to Alexa

555 (#4413, Cell Signaling) and anti-mouse conjugated to peroxidase (#AP124P, Millipore) both diluted 1:500] were used. After rinses in wash buffer (prepared according to the manufacturer's protocol), slices were incubated for 10 min in TSA plus Cy5 system (1:300 in amplification buffer provided by the manufacturer, #FP1117, Perkin Elmer). Slices obtained from *TGR5^{f/f}*-AAV-GFAP-Cre-mCherry/*TGR5^{f/f}*-AAV-GFAP-mCherry mice were incubated in the rabbit antiserum against GFAP and then in a goat anti-rabbit secondary antibody conjugated to Alexa 647 (1:500, #4414, Cell Signaling). Then slices were treated according to the manufacturer's instructions of the Mouse on Mouse Fluorescein kit (#FMK-2201, Vector Laboratories) to reveal the S100β staining. Briefly, slices were incubated in an Avidin/Biotin blocking kit (#SP-2001, Vector Laboratoires), 1h in a proprietary Mouse IgG blocking reagent, 30 min in the monoclonal mouse antibody against S100β (see above, 1:1000 in the manufacturer's diluent), 10 min in a mouse on mouse (M.O.M.™, Vector) Biotinylated Anti-Mouse Ig Reagent and 5 min in a cell sorter grade of Fluorescein Avidin D.

Images were acquired on a Leica DM6 CFS TCS SP8 confocal microscope using an objective 10X (voxel size: 1.0823x1.0823x4.2839 µm^3) or an objective 40X (voxel size: 0.2705x0.2705x0.3462µm^3). Laser diodes used were at 405 nm (DAPI), 488 nm (Alexa 488 or Flurorescein or GFP), 552 nm (Alexa 555 or mCherry) and 638 nm (Alexa 647 or Cy5). Parameters were determined at the beginning of the acquisition and were maintained for all acquisitions of the same experiment. All presented images are Z projection (maximal intensity) of a given stack.

Fluorescent in situ hybridization combined with IHC

Perfused brain slices from 5 $TGR5^{f/f}$ mice receiving the AAV-Cag-Cre-GFP were used. Digoxigenin-labeled riboprobe against the glutamatergic marker vesicular glutamate transporter 2 (*vGlut2*) and the GABAergic marker GABA synthesizing enzyme GAD65 (corresponding to the gene *GAD2*) were obtained as previously described (Saucisse et al., 2020). Free-floating sections were treated with 0.2M HCl then acetylated with 0.25% acetic anhydride in 0.1 M triethanolamine, pH=8.0 for 10 min. Between all steps, sections were rinsed in PBS with 0.01% diethylpyrocarbonate. VGlut2-DIG or GAD65-DIG was dissolved 1/1000 in hybmix solution (50% deionized formamide, 20mM Tris at pH=8.0, 300mM NaCl, 5mM EDTA, 10% dextran sulfate, 1X Denhardt's solution, 0.5mg/mL tRNA, 0.2mg/mL acid-cleaved carrier DNA from salmon's sperm, 1M DTT dissolved in water containing 0.01% DEPC) and linearized by heating at 90°C for 5 min. After hybridization overnight at 70°C, sections were washed at 70°C with increased stringency buffers (5X saline sodium citrate (SSC) for 5min, 2X SSC + 50% Formamide amide, 1X SSC + 50% Formamide amide and 0.1X SSC for 30min each, with 0.1% Tween20 added to each buffer). Sections were incubated 30 min in 3% H_2O_2 in TNT (100mM Tris-HCl, 150mM NaCl, 0.05% Tween20) to quench endogenous peroxydases, 20 min in 0.2M HCl, 1h in blocking buffer (#FP1012; Akoya Biosciences), 2h in antidigoxigenin-POD antibody (1:1500 in the blocking buffer; #11207733910; Roche), 30 min in TSA plus Cy3 system (1:100 in 1X Plus amplification buffer provided by the manufacturer; #NEL744001KT; Akoya Biosciences), 30 min in 3% H_2O_2 TNT to block HRP and overnight at 4°C in goat anti-GFP antibody (1/:400 in PBST; #AB0066-200; Sicgen). Between all steps, sections were rinsed in TNT. After 3 washes in PBS, slices were incubated 2h in a donkey anti-goat secondary antibody conjugated to Alexa 488 (1:500 in PBST; #A11055; Life technologies). After 3 washes in PBS, slices were

stained for 5 min with DAPI (1:20 000, in PBS), washed in 50mM Tris (pH=7.5), mounted on gelatinized slides, cover-slipped using Prolong® and kept at 4°C until use. All steps were carried out at room temperature unless stated otherwise.

Confocal images of the medio-basal hypothalamus were collected using a Leica DMi6000 TCS SP8 X confocal microscope (Leica microsystems, Germany) enabled with a 20X/NA 0.75 oil immersion objective (Leica HC PL APO CS2), a laser diode at 405nm (DAPI), a white light excitation laser (set at 499nm for AF488 and at 553nm for Cy3) and hybrid detectors. Images were corrected automatically for brightness and contrast, and analyzed using ImageJ (NIH, USA). For each image, we used the plugin Cell counter in ImageJ to select and count GFP positive cells that co-expressed (or not) *vGlut2* or *GAD65*. The analysis was made on 2-8 medio-basal hypothalami from 2-4 sections per animal. For illustration purposes, some images were also taken with a 63X/NA 1.4 oil objective.

Transient transfection reporter assay

Murine TGR5 activation with the BA mix and the subsequent increase in intracellular cAMP was measured using a luciferase reporter gene assay.

HEK-293 cells were transiently co-transfected with pCMV AC6-TGR5m expression plasmid (Lasalle et al., 2017) and the pCRE TALuciferase reporter plasmid using the JET PEI reagent (Polyplus transfection). The pCMV-β-galactosidase expression plasmid was co-transfected as a control for transfection efficiency. Transfected cells were seeded in 96-well plates and incubated overnight in triplicate with the compounds at

increasing concentrations. LCA at 10 µM was used as a positive reference compound. At the end of the experiment, cells were washed once with ice-cold PBS, and the luciferase and β-galactosidase assays were performed. Luciferase activity was then normalized to internal control β-galactosidase activity, as done in (Staels et al., 1998). Luminescence was measured with a Mithras plate reader (Berthold). Data were expressed as the percentage of the 10 µM LCA value, and half maximal effective concentration (EC_{50}) was calculated using Prism software. Dose-response curves were fitted by a nonlinear regression analysis to a 4 parameter logistic equation.

QUANTIFICATION AND STATISTICAL ANALYSIS

Statistical analysis was carried out using the GraphPad Prism Software version 8.0 for Windows (La Jolla, CA, USA). Data are expressed as mean ± S.E.M. Sample sizes for experiments were determined based on sample sizes used in similar experiments reported previously in the literature.

The statistical test used for each comparison is described in the figure legends corresponding to the specific figure and further detailed in table S1. Briefly, when comparing 2 groups, data were analyzed by an unpaired Student's t-test (Shapiro-Wilk test for normality when small sample sizes, otherwise, Kolmogorov-Smirnov test for normality), or a Mann-Whitney U test (nonparametric). When comparing 3 or more groups, data were analyzed by one-way ANOVA. Two-way ANOVAs were performed for analyzing body weight, body composition, cumulative food intake and feed efficiency considering genotype (with or without hypothalamic deletion of *TGR5*) and diet (HFD or

HFD+CA) as factors. Body weight, insulin tolerance test, food intake, energy expenditure, RER, meal size, and locomotor activity over time were analyzed by two-way repeated measures ANOVA considering treatment and time as factors. For analyzing energy expenditure at 22°C or at 30°C, a three-way ANOVA was carried out considering time of day (day or night), treatment (Vehicle or CCDC) and temperature (22°C or 30°C) as factors. Similarly, a three-way ANOVA was carried out for analyzing body weight and food intake over time on *TGR5^{f/f}* mice receiving AAV-Cag-Cre-GFP or its control that were either exposed to a HFD or a HFD+CA, considering time, genotype and diet as factors. Fisher's LSD post-hoc tests were run when applicable for identifying differences amongst groups. In all cases, tests were considered significant when $p<0.05$.

Supplemental information

Supplemental information includes 4 tables and 5 figures.

Table S1. Statistical analyses for main and supplementary figures (Related to STAR Methods).

References

Bellocchio, L., Soria-Gomez, E., Quarta, C., Metna-Laurent, M., Cardinal, P., Binder, E., Cannich, A., Delamarre, A., Haring, M., Martin-Fontecha, M., Vega, D., Leste-Lasserre, T., Bartsch, D., Monory, K., Lutz, B., Chaouloff, F., Pagotto, U., Guzman, M., Cota, D., and Marsicano, G. (2013). Activation of the sympathetic nervous system mediates hypophagic and anxiety-like effects of CB(1) receptor blockade. Proc Natl Acad Sci U S A *110*, 4786-4791.

Blaszkiewicz, M., and Townsend, K.L. (2016). Adipose Tissue and Energy Expenditure: Central and Peripheral Neural Activation Pathways. Curr Obes Rep *5*, 241-250.

Broeders, E.P., Nascimento, E.B., Havekes, B., Brans, B., Roumans, K.H., Tailleux, A., Schaart, G., Kouach, M., Charton, J., Deprez, B., Bouvy, N.D., Mottaghy, F., Staels, B., van Marken Lichtenbelt, W.D., and Schrauwen, P. (2015). The Bile Acid Chenodeoxycholic Acid Increases Human Brown Adipose Tissue Activity. Cell Metab *22*, 418-426.

Cardinal, P., Andre, C., Quarta, C., Bellocchio, L., Clark, S., Elie, M., Leste-Lasserre, T., Maitre, M., Gonzales, D., Cannich, A., Pagotto, U., Marsicano, G., and Cota, D. (2014). CB1 cannabinoid receptor in SF1-expressing neurons of the ventromedial hypothalamus determines metabolic responses to diet and leptin. Mol Metab *3*, 705-716.

Clapham, J.C. (2012). Central control of thermogenesis. Neuropharmacology *63*, 111-123.

Dietrich, M.O., and Horvath, T.L. (2013). Hypothalamic control of energy balance: insights into the role of synaptic plasticity. Trends Neurosci *36*, 65-73.

Doignon, I., Julien, B., Serriere-Lanneau, V., Garcin, I., Alonso, G., Nicou, A., Monnet, F., Gigou, M., Humbert, L., Rainteau, D., Azoulay, D., Castaing, D., Gillon, M.C., Samuel, D., Duclos-Vallee, J.C., and Tordjmann, T. (2011). Immediate neuroendocrine signaling after partial hepatectomy through acute portal hyperpressure and cholestasis. J Hepatol *54*, 481-488.

Evans, K.A., Budzik, B.W., Ross, S.A., Wisnoski, D.D., Jin, J., Rivero, R.A., Vimal, M., Szewczyk, G.R., Jayawickreme, C., Moncol, D.L., Rimele, T.J., Armour, S.L., Weaver, S.P., Griffin, R.J., Tadepalli, S.M., Jeune, M.R., Shearer, T.W., Chen, Z.B., Chen, L., Anderson, D.L., Becherer, J.D., De Los Frailes, M., and Colilla, F.J. (2009). Discovery of 3-aryl-4-isoxazolecarboxamides as TGR5 receptor agonists. J Med Chem *52*, 7962-7965.

García-Cáceres, C., Balland, E., Prevot, V., Luquet, S., Woods, S.C., Koch, M., Horvath, T.L., Yi, C.X., Chowen, J.A., Verkhratsky, A., Araque, A., Bechmann, I., Tschöp, M.H. (2019). Role of astrocytes, microglia, and tanycytes in brain control of systemic metabolism. Nat Neurosci *22*, 7-14.

Garcia-Canaveras, J.C., Donato, M.T., Castell, J.V., and Lahoz, A. (2012). Targeted profiling of circulating and hepatic bile acids in human, mouse, and rat using a UPLC-MRM-MS-validated method. J Lipid Res *53*, 2231-2241.

Hassouna, R., Zizzari, P., Viltart, O., Yang, S.K., Gardette, R., Videau, C., Badoer, E., Epelbaum, J., Tolle, V. (2012). A natural variant of obestatin, Q90L, inhibits ghrelin's action on food intake and GH secretion and targets NPY and GHRH neurons in mice. PLoS One *7*, e51135.

Hebert-Chatelain, E., Desprez, T., Serrat, R., Bellocchio, L., Soria-Gomez, E., Busquets-Garcia, A., Pagano Zottola, A.C., Delamarre, A., Cannich, A., Vincent, P., Varilh, M., Robin, L.M., Terral, G., Garcia-Fernandez, M.D., Colavita, M., Mazier, W., Drago, F., Puente, N., Reguero, L., Elezgarai, I., Dupuy, J.W., Cota, D., Lopez-Rodriguez, M.L., Barreda-Gomez, G., Massa, F., Grandes, P., Benard, G., and Marsicano, G. (2016). A cannabinoid link between mitochondria and memory. Nature *539*, 555-559.

Higashi, T., Watanabe, S., Tomaru, K., Yamazaki, W., Yoshizawa, K., Ogawa, S., Nagao, H., Minato, K., Maekawa, M., and Mano, N. (2017). Unconjugated bile acids in rat brain: Analytical method based on LC/ESI-MS/MS with chemical derivatization and estimation of their origin by comparison to serum levels. Steroids *125*, 107-113.

Jensen, D.D., Godfrey, C.B., Niklas, C., Canals, M., Kocan, M., Poole, D.P., Murphy, J.E., Alemi, F., Cottrell, G.S., Korbmacher, C., Lambert, N.A., Bunnett, N.W., and Corvera, C.U. (2013). The bile acid receptor TGR5 does not interact with beta-arrestins or traffic to endosomes but transmits sustained signals from plasma membrane rafts. J Biol Chem *288*, 22942-22960.

Kaiyala, K.J., and Schwartz, M.W. (2011) Toward a more complete (and less controversial) understanding of energy expenditure and its role in obesity pathogenesis. Diabetes *60*, 17-23.

Kawamata, Y., Fujii, R., Hosoya, M., Harada, M., Yoshida, H., Miwa, M., Fukusumi, S., Habata, Y., Itoh, T., Shintani, Y., Hinuma, S., Fujisawa, Y., and Fujino, M. (2003). A G protein-coupled receptor responsive to bile acids. J Biol Chem *278*, 9435-9440.

Keitel, V., Gorg, B., Bidmon, H.J., Zemtsova, I., Spomer, L., Zilles, K., and Haussinger, D. (2010). The bile acid receptor TGR5 (Gpbar-1) acts as a neurosteroid receptor in brain. Glia *58*, 1794-1805.

Kuipers, F., Bloks, V.W., and Groen, A.K. (2014). Beyond intestinal soap--bile acids in metabolic control. Nat Rev Endocrinol *10*, 488-498.

Kumar, D.P., Rajagopal, S., Mahavadi, S., Mirshahi, F., Grider, J.R., Murthy, K.S., and Sanyal, A.J. (2012). Activation of transmembrane bile acid receptor TGR5 stimulates insulin secretion in pancreatic beta cells. Biochem Biophys Res Commun *427*, 600-605.

Lasalle, M., Hoguet, V., Hennuyer, N., Leroux, F., Piveteau, C., Belloy, L., Lestavel, S., Vallez, E., Dorchies, E., Duplan, I., Sevin, E., Culot, M., Gosselet, F., Boulahjar, R., Herledan, A., Staels, B., Deprez, B., Tailleux, A., and Charton, J. (2017). Topical Intestinal Aminoimidazole Agonists of G-Protein-Coupled Bile Acid Receptor 1 Promote Glucagon Like Peptide-1 Secretion and Improve Glucose Tolerance. J Med Chem *60*, 4185-4211.

Liu, S., Marcelin, G., Blouet, C., Jeong, J.H., Jo, Y.H., Schwartz, G.J., and Chua, S., Jr. (2018). A gut-brain axis regulating glucose metabolism mediated by bile acids and competitive fibroblast growth factor actions at the hypothalamus. Mol Metab *8*, 37-50.

Maruyama, T., Tanaka, K., Suzuki, J., Miyoshi, H., Harada, N., Nakamura, T., Miyamoto, Y., Kanatani, A., and Tamai, Y. (2006). Targeted disruption of G protein-coupled bile acid receptor 1 (Gpbar1/M-Bar) in mice. J Endocrinol *191*, 197-205.

McMillin, M., Frampton, G., Tobin, R., Dusio, G., Smith, J., Shin, H., Newell-Rogers, K., Grant, S., and DeMorrow, S. (2015). TGR5 signaling reduces neuroinflammation during hepatic encephalopathy. J Neurochem *135*, 565-576.

Mertens, K.L., Kalsbeek, A., Soeters, M.R., and Eggink, H.M. (2017). Bile Acid Signaling Pathways from the Enterohepatic Circulation to the Central Nervous System. Front Neurosci *11*: 617.

Ockenga, J., Valentini, L., Schuetz, T., Wohlgemuth, F., Glaeser, S., Omar, A., Kasim, E., duPlessis, D., Featherstone, K., Davis, J.R., Tietge, U.J., Kroencke, T., Biebermann, H., Kohrle, J., and Brabant, G. (2012). Plasma bile acids are associated with energy expenditure and thyroid function in humans. J Clin Endocrinol Metab *97*, 535-542.

Parry, G.J., Rodrigues, C.M., Aranha, M.M., Hilbert, S.J., Davey, C., Kelkar, P., Low, W.C., and Steer, C.J. (2010). Safety, tolerability, and cerebrospinal fluid penetration of ursodeoxycholic Acid in patients with amyotrophic lateral sclerosis. Clin Neuropharmacol *33*, 17-21.

Patti, M.E., Houten, S.M., Bianco, A.C., Bernier, R., Larsen, P.R., Holst, J.J., Badman, M.K., Maratos-Flier, E., Mun, E.C., Pihlajamaki, J., Auwerx, J., and Goldfine, A.B. (2009). Serum bile acids are higher in humans with prior gastric bypass: potential contribution to improved glucose and lipid metabolism. Obesity (Silver Spring) *17*, 1671-1677.

Perino, A., Demagny, H., Velazquez-Villegas, L.A., and Schoonjans, K. (2020). Molecular Physiology of Bile Acid Signaling in Health, Disease and Aging. Physiol Rev. doi: 10.1152/physrev.00049.2019.

Perino, A., Pols, T.W., Nomura, M., Stein, S., Pellicciari, R., and Schoonjans, K. (2014). TGR5 reduces macrophage migration through mTOR-induced C/EBPbeta differential translation. J Clin Invest *124*, 5424-5436.

Quarta, C., Bellocchio, L., Mancini, G., Mazza, R., Cervino, C., Braulke, L.J., Fekete, C., Latorre, R., Nanni, C., Bucci, M., Clemens, L.E., Heldmaier, G., Watanabe, M., Leste-Lassere, T., Maitre, M., Tedesco, L., Fanelli, F., Reuss, S., Klaus, S., Srivastava, R.K., Monory, K., Valerio, A., Grandis, A., De Giorgio, R., Pasquali, R., Nisoli, E., Cota, D., Lutz, B., Marsicano, G., and Pagotto, U. (2010). CB(1) signaling in forebrain and sympathetic neurons is a key determinant of endocannabinoid actions on energy balance. Cell Metab *11*, 273-285.

Saucisse, N., Mazier, W., Simon, V., Binder, E., Catania., C., Bellocchio, L., Romanov, R.A., Matias,I., Zizzari, P., Leon, S., Quarta, C., Cannich, A., Meece, K., Gonzales, D., Clark, S., Becker, J.M., Yeo, G.S.H., Merkle F.T., Wardlaw S.L., Harkany, T., Massa, F., Marsicano, G., and Cota, D. (2020). POMC neurons functional heterogeneity relies on mTORC1 signaling. bioRxiv 2020.03.25.007765; doi:10.1101/2020.03.25.007765.

Schwenk, F., Baron, U., and Rajewsky, K. (1995). A cre-transgenic mouse strain for the ubiquitous deletion of loxP-flanked gene segments including deletion in germ cells. Nucleic Acids Res *23*, 5080-5081.

Simonen, M., Dali-Youcef, N., Kaminska, D., Venesmaa, S., Kakela, P., Paakkonen, M., Hallikainen, M., Kolehmainen, M., Uusitupa, M., Moilanen, L., Laakso, M., Gylling, H., Patti, M.E., Auwerx, J., and Pihlajamaki, J. (2012). Conjugated bile acids associate with altered rates of glucose and lipid oxidation after Roux-en-Y gastric bypass. Obes Surg *22*, 1473-1480.

Song, P., Zhang, Y., and Klaassen, C.D. (2011). Dose-response of five bile acids on serum and liver bile Acid concentrations and hepatotoxicty in mice. Toxicol Sci *123*, 359-367.

Staels, B., Koenig, W., Habib, A., Merval, R., Lebret, M., Torra, I.P., Delerive, P., Fadel, A., Chinetti, G., Fruchart, J.C., Najib, J., Maclouf, J., and Tedgui, A. (1998). Activation of human aortic smooth-muscle cells is inhibited by PPARalpha but not by PPARgamma activators.Nature *393*:790-793.

Teodoro, J.S., Zouhar, P., Flachs, P., Bardova, K., Janovska, P., Gomes, A.P., Duarte, F.V., Varela, A.T., Rolo, A.P., Palmeira, C.M., and Kopecky, J. (2014). Enhancement of brown fat thermogenesis using chenodeoxycholic acid in mice. Int J Obes (Lond) *38,* 1027-1034.

Thomas, C., Gioiello, A., Noriega, L., Strehle, A., Oury, J., Rizzo, G., Macchiarulo, A., Yamamoto, H., Mataki, C., Pruzanski, M., Pellicciari, R., Auwerx, J., and Schoonjans, K. (2009). TGR5-mediated bile acid sensing controls glucose homeostasis. Cell Metab *10*, 167-177.

Tremaroli, V., Karlsson, F., Werling, M., Ståhlman, M., Kovatcheva-Datchary, P., Olbers, T., Fändriks, L., le Roux, C.W., Nielsen, J., and Bäckhed, F. (2015). Roux-en-Y Gastric Bypass and Vertical Banded Gastroplasty Induce Long-Term Changes on the Human Gut Microbiome Contributing to Fat Mass Regulation. Cell Metab *22*, 228-238.

Vaughan, C.H., Zarebidaki, E., Ehlen, J.C., and Bartness, T.J. (2014). Analysis and measurement of the sympathetic and sensory innervation of white and brown adipose tissue. Methods Enzymol *537*, 199-225.

Velazquez-Villegas, L.A., Perino, A., Lemos, V., Zietak, M., Nomura, M., Pols, T.W.H., and Schoonjans, K. (2018). TGR5 signalling promotes mitochondrial fission and beige remodelling of white adipose tissue. Nat Commun *9*, 245.

Watanabe, M., Houten, S.M., Mataki, C., Christoffolete, M.A., Kim, B.W., Sato, H., Messaddeq, N., Harney, J.W., Ezaki, O., Kodama, T., Schoonjans, K., Bianco, A.C., and Auwerx, J. (2006). Bile acids induce energy expenditure by promoting intracellular thyroid hormone activation. Nature *439*, 484-489.

Wu, X., Li, J.Y., Lee, A., Lu, Y.X., Zhou, S.Y., and Owyang, C. (2020). Satiety induced by bile acids is mediated via vagal afferent pathways. JCI Insight *5*.

Zietak, M., and Kozak, L.P. (2016). Bile acids induce uncoupling protein 1-dependent thermogenesis and stimulate energy expenditure at thermoneutrality in mice. Am J Physiol Endocrinol Metab *310*, E346-354.

Zuo, G., Zhang, T., Huang, L., Araujo, C., Peng, J., Travis, Z., Okada, T., Ocak, U., Zhang, G., Tang, J., Lu, X., and Zhang, J.H. (2019). Activation of TGR5 with INT-777 attenuates oxidative stress and neuronal apoptosis via cAMP/PKCepsilon/ALDH2 pathway after subarachnoid hemorrhage in rats. Free Radic Biol Med *143*, 441-453.

Figure 1
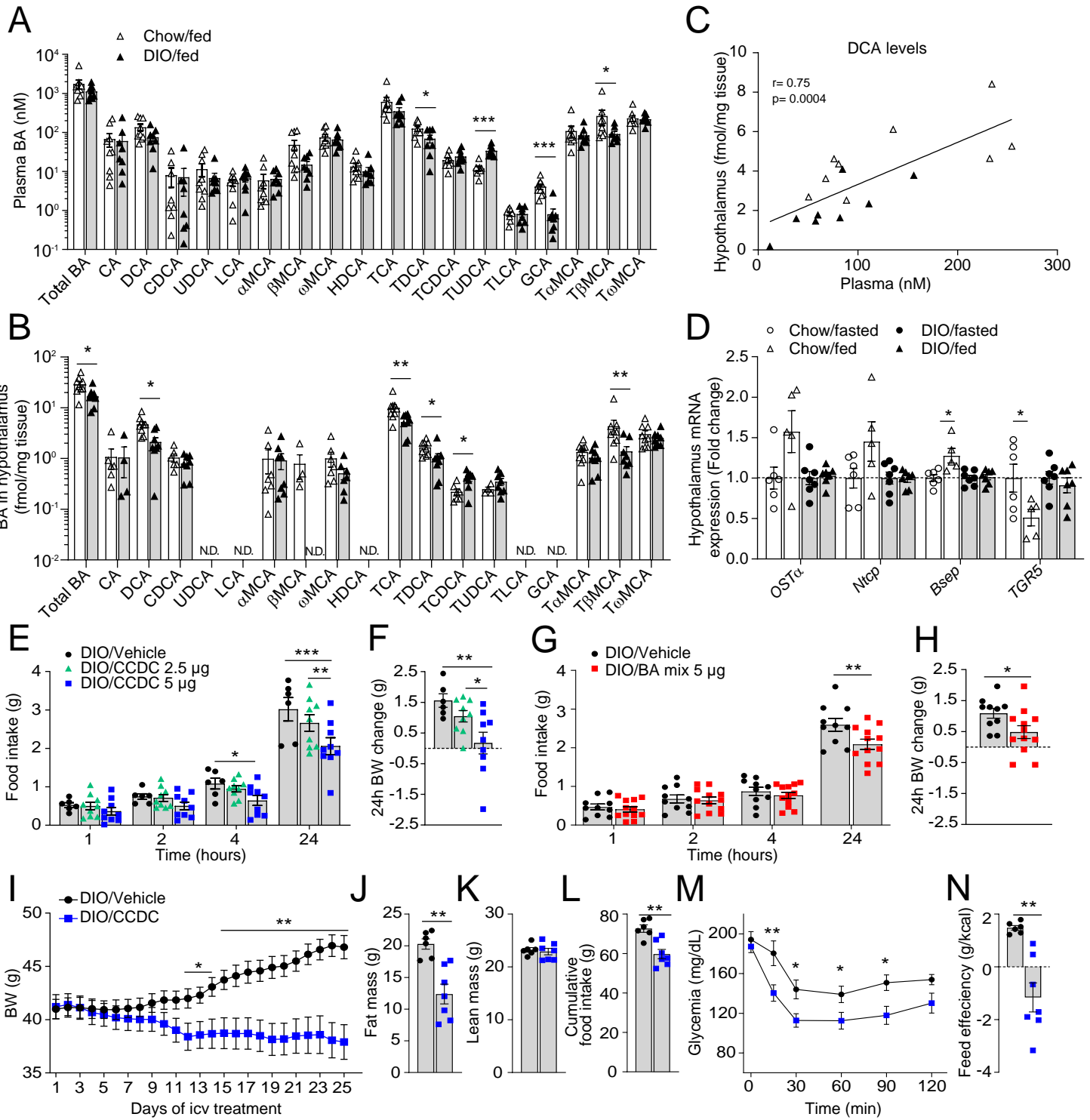
Figure 2

Figure 3

Figure 4

A

TGR5^{fl}-AAV-Cag-GFP HFD
TGR5^{fl}-AAV-Cag-GFP HFD+CA
TGR5^{fl}-AAV-Cag-Cre-GFP HFD
TGR5^{fl}-AAV-Cag-Cre-GFP HFD+CA

AAV
HFD±CA
chow
BW (g)
Days
###
###

B
CA-induced BW change (%HFD-control)
GFP   Cre
**

C
CA-induced fat mass change (%HFD-control)
GFP   Cre
***

D
CA-induced food intake change (%HFD-control)
GFP   Cre

E
CA-induced feed efficiency change (%HFD-control)
GFP   Cre
**
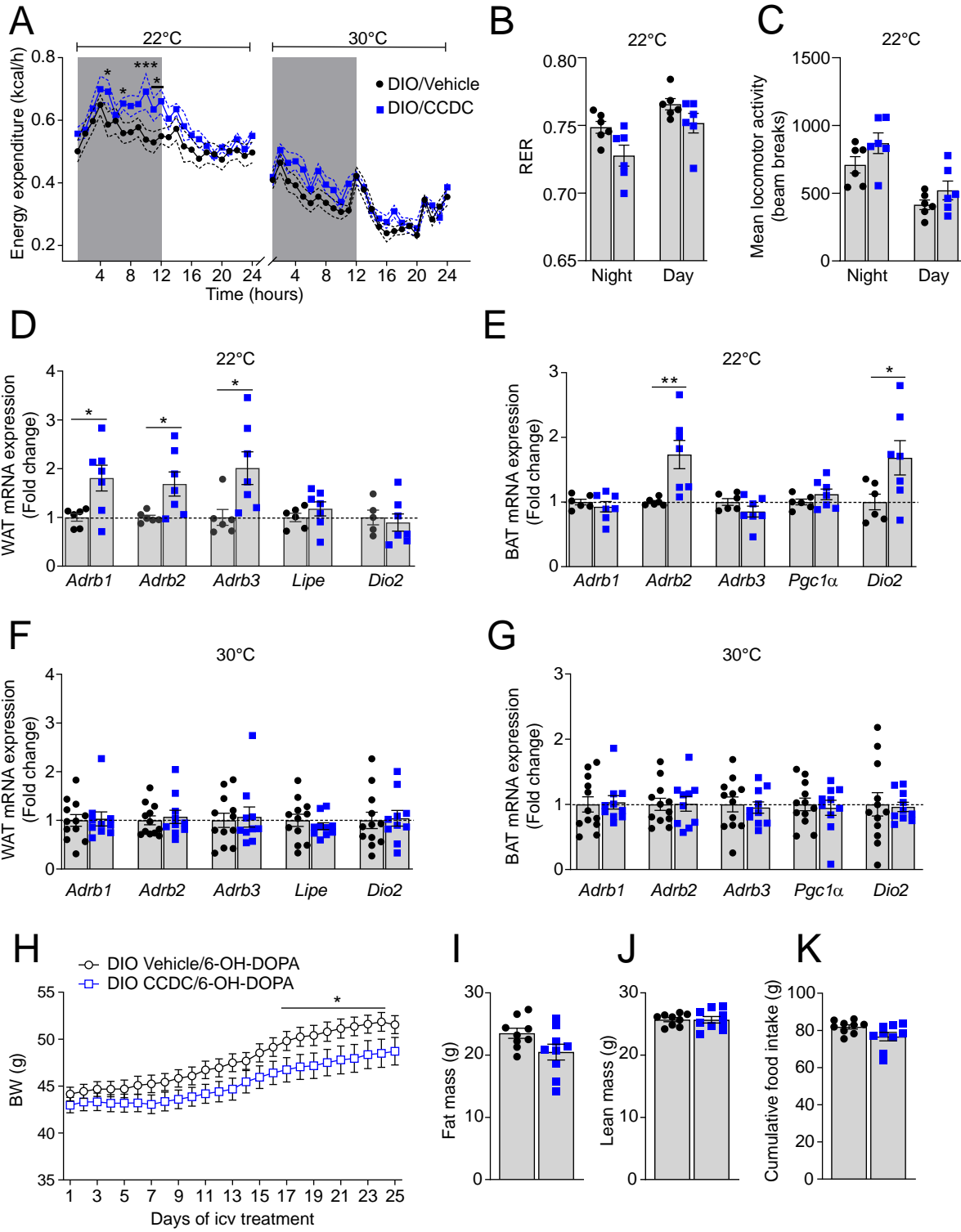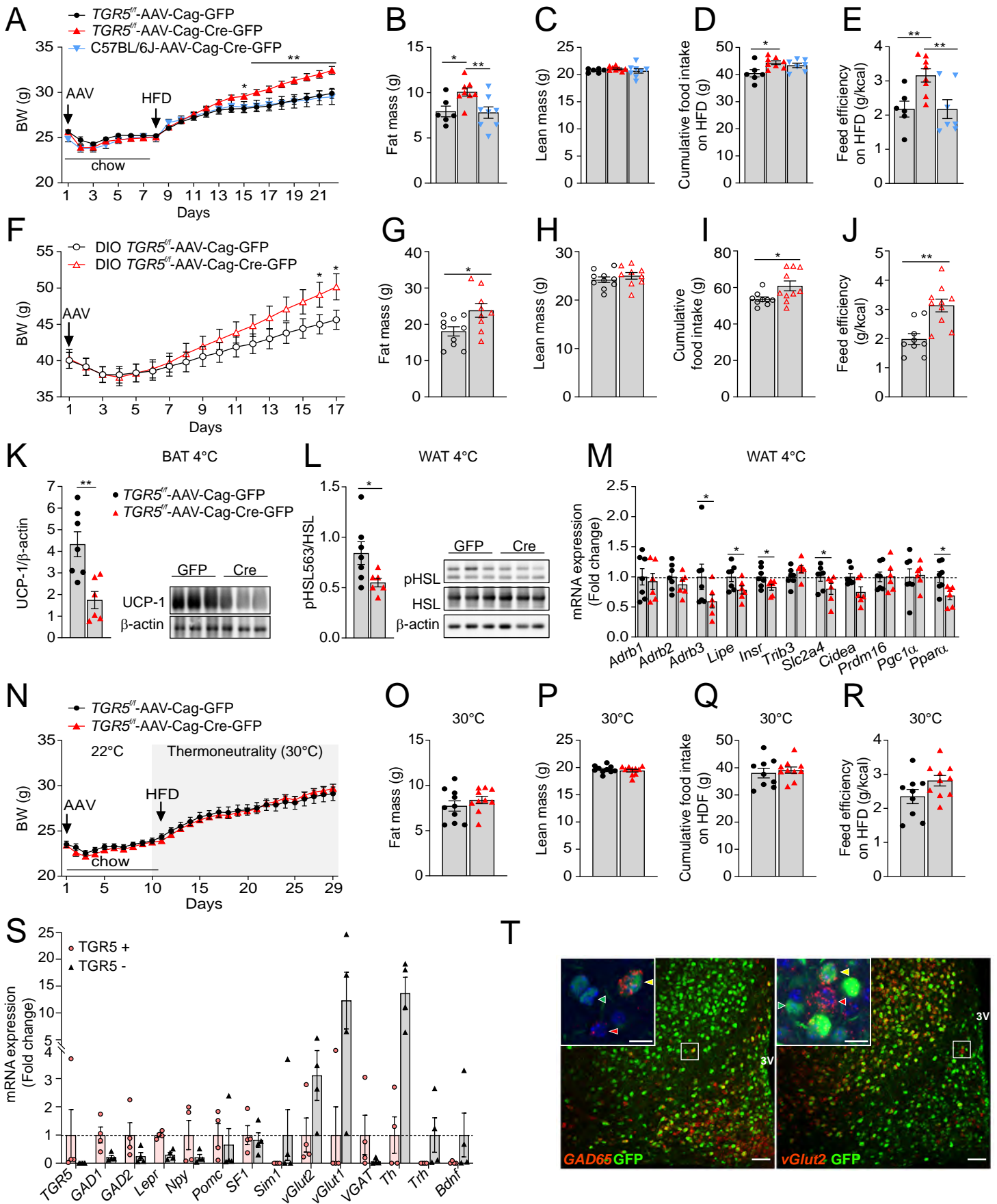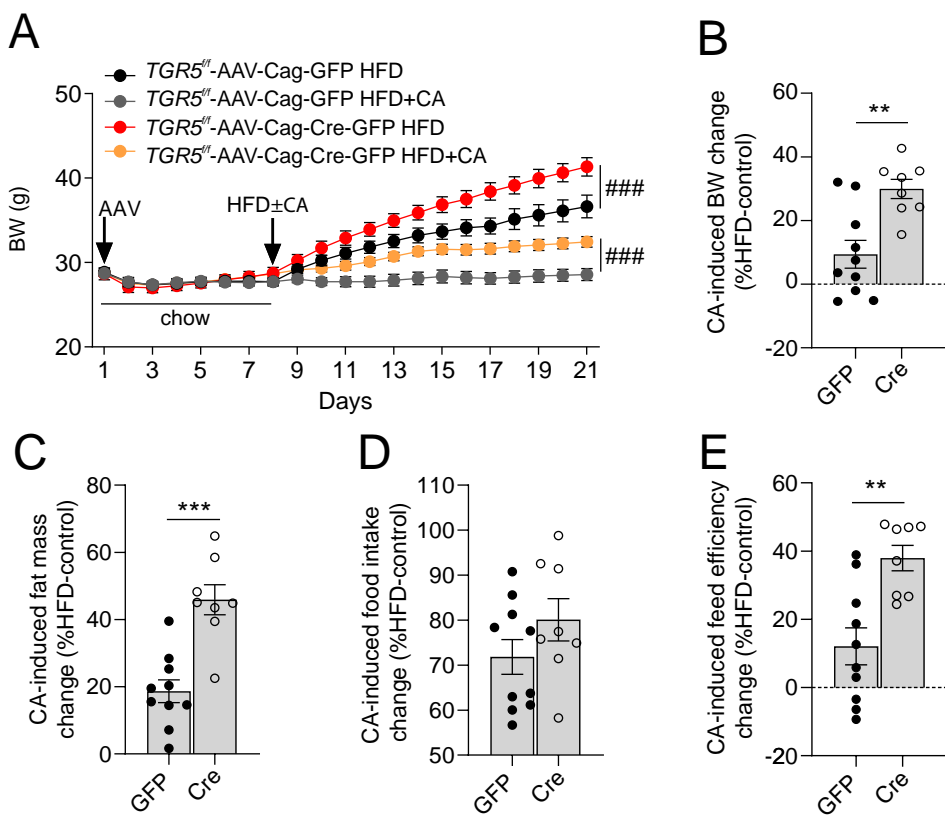
Key Resources Table

REAGENT or RESOURCE	SOURCE	IDENTIFIER
Antibodies		
Alexa Fluor 594 Donkey anti-rabbit IgG	Jackson ImmunoResearch Labs	Cat# 711-585-152; RRID:AB_2340621
Goat anti-Biotin, HRP linked antibody	Cell Signaling	Cat# 7075; RRID:AB_10696897
Goat anti-mouse IgG conjugated to peroxidase	Millipore	Cat# AP124P; RRID:AB_90456
Alexa Fluor 555 goat anti-rabbit IgG	Cell Signaling Technology	Cat# 4413; RRID:AB_10694110
Anti-Rabbit IgG,HRP linked antibody	Cell Signaling	Cat# 7074; RRID:AB_2099233
Alexa Fluor 647 Donkey anti-chicken IgG	Jackson ImmunoResearch Labs	Cat# 703-606-155; RRID:AB_2340380
Alexa Fluor 488 Donkey anti-goat IgG	Life technologies	Cat#A11055 RRID:AB_2534102
Alexa Fluor 448 Donkey anti-rabbit IgG	Jackson ImmunoResearch Labs	Cat# 711-545-152; RRID:AB_2313584
Alexa Fluor 647 Goat anti-rabbit IgG	Cell Signaling Technology	Cat# 4414; RRID:AB_10693544
Goat polyclonal anti-GFP	Sicgen	Cat#AB0066-200 RRID:AB_2333101
Mouse monoclonal anti-S100β-subunit (clone SH-B1)	Sigma-Aldrich	Cat# S2532; RRID:AB_477499
Rabbit polyclonal anti-GFAP	Agilent	Cat# Z0334; RRID:AB_10013382
Rabbit polyclonal anti-β-actin	Cell Signaling	Cat# 4967; RRID:AB_330288
Rabbit polyclonal anti-HSL	Cell Signaling	Cat# 4107; RRID:AB_2296900
Rabbit polyclonal anti-phospho-HSL ser563	Cell Signaling	Cat# 4139; RRID:AB_2135495
Rabbit polyclonal anti-TH	Millipore	Cat# 152; RRID:AB_390204
Rabbit polyclonal anti UCP-1	Abcam	Cat# 10983; RRID:AB_2241462
Sheep Anti-Digoxigenin Fab fragments Antibody, POD Conjugated	Roche	Cat#11207733910 RRID:AB_514500
Chicken polyclonal anti-NeuN	Millipore	Cat# ABN91; RRID:AB_11205760
Rabbit polyclonal anti-iba-1	Wako	Cat# 019-19741; RRID:AB_839504
Bacterial and Virus Strains		
AAV1/2-Cre-CAG-hrGFP	(Hebert-Chatelain et al., 2016)	Virus n°1 lab stock
AAV1/2-Cag-hrGFP	(Hebert-Chatelain et al., 2016)	Virus n°4 lab stock

ssAAV-2-hGFAP-mCherry_iCre-WPRE-hGHp(A)	Viral Vector Facility	v233; iCre: Addgene # 24593; hGFAP promoter fragment: DOI: 10.1002/glia.20622
ssAAV-2-hGFAP-mCherry-WPRE-hGHp(A)	Viral Vector Facility	v222; hGFAP promoter fragment: DOI: 10.1002/glia.20622
pAAV-hSyn-DIO-mCherry	Addgene	#50459-AAV8
Chemicals, Peptides, and Recombinant Proteins		
3-(2-chlorophenyl)-N-(4-chlorophenyl)-N, 5-dimethylisoxazole-4-carboxamide (CCDC)	Abcam	Cat# ab142091
Biotinylated protein ladder	Cell Signaling	Cat# 7727
Color prestained protein standard, broad range	New England Biolabs	Cat# P7712
sodium salts of taurocholic, glycocholic, deoxycholic, and cholic acids (BA mix)	Sigma-Aldrich	Cat#S9875
6-Hydroxydopamine hydrochloride (6-OH-DOPA)	Sigma-Aldrich	Cat# H4381
DAPI (4',6'-diamidino-2-phenylindol)	Molecular Probes	Cat# D1306
Enhanced chemiluminescence Plus (ECL Plus)	Perkin Elmer	Cat# NEL-103E001EA
Neuropeptide Y (Human, Rat, Mouse)	Phoenix Pharmaceuticals Inc.	Cat# 049-03
Prolong gold antifade	Vector Laboratories	Cat# P36930
Radioimmunoprecipitation assay lysis buffer (RIPA) system	Santa Cruz Biotechnology	Cat# SC-24948
TSA plus Cy3 system	Akoya Biosciences	Cat#NEL744001KT
TSA plus Cy5 system	Perkin Elmer	Cat# FP1117
Umulin Rapide (Human insulin)	Lilly	Cat# HI-0210
Critical Commercial Assays		
Avidin/Biotin blocking kit	Vector Laboratoires	Cat# SP-2001
DNA5k kit	Perkin Elmer	CLS760675; chip # 760527
GoTaq G2 Hot Start Green Master Mix	Promega	M7423
NucleoSpin kit	Macherey-Nagel	740454.4
Mouse on Mouse Fluorescein kit	Vector Laboratories	Cat# FMK-2201
Pierce BSA Protein Assay kit	Thermo Fisher Scientific	Cat# 23225
Maxima Reverse Transcriptase kit	Fisher Scientific	10420100
Experimental Models: Cell lines		
HEK293	ATCC	CRL-1573
Experimental Models: Organisms/Strains		
Mouse C57BL/6J	Charles River	N/A
Mouse $Gpbar1^{tm1.1Auw}$	(Thomas et al., 2009)	MGI:4359382
Mouse B6.C-Tg(CMV-cre)1Cgn/J	The Jackson Laboratory	stock #006054
Mouse $Slc17a6^{tm2(cre)Lowl}$/J	The Jackson Laboratory	stock # 016963
Mouse B6J.129S6(FVB)-$Slc32a1^{tm2(cre)Lowl}$/MwarJ	The Jackson Laboratory	stock # 028862
Mouse B6-$Gpbar1^{tm1Ciphe}$	This paper	N/A

Oligonucleotides		
qPCR primers for several tissues and cells, see **Table S4**	This paper	N/A
PCR primer used for genotyping P711-*TGR5* lox GGGACAGCACATTATCACTGAGGC	(Thomas et al., 2009)	N/A
PCR primer used for genotyping P712-*TGR5* lox GGAACAGAGCACTCTGTGACTTCC	(Thomas et al., 2009)	N/A
PCR primer used for genotyping P786-*TGR5* lox TGGGTGAGTGGAGTCTTCCT	Eurogentec	Custom
Software and Algorithms		
ImageJ	NIH	N/A
Prism	GraphPad Software	https://www.graphpad.com/
PhenoMaster Software	TSE System	https://www.tse-systems.com/product-details/phenomaster
Other		
Brain infusion kit III	Alzet	N/A
Cannulas, dummy	Plastics One	C313DCS-5/SPO
Cannulas, guide	Plastics One	C313GS-5/SP 22GA
Cannulas, internal injector	Plastics One	C313IS-5/SPC 28GA
Glucometer	One Touch	Verio Flex
Glucose strips	One Touch	Verio
High-fat diet 60% Kcal from fat with 0.5% sodium cholate	Research Diets	D07033001
High-fat diet 60% Kcal from fat	Research Diets	D12492
Standard chow diet	SAFE Diets	A03; U8200G10R
Metabolic chambers	TSE System	N/A
Micro-osmotic pumps	Alzet	Model 1004
EchoMRI 900	Echo Medical Systems, Houston, TX	N/A

Figure S1. Acute and chronic central effects of a selective TGR5 agonist in DIO mice (Related to Figure 1).

(A) *In vitro* dose-response profiles of the BA mix in transient transfection reporter assay. LCA at 10 µM was used as a positive control for murine TGR5 activation. Cells were incubated overnight in the presence of indicated concentrations of BA mix or positive LCA control. Luciferase activity was measured and normalized to internal control β-galactosidase activity. Data are expressed as the percentage of the 10 µM LCA value. Efficacy: E_{max} is the maximal TGR5 fold activation expressed relative to the activation obtained with LCA (10 µM) set at 100%. EC_{50}: effective concentration inducing 50% of E_{max}. The BA mix had an E_{max} of 80% at 30µM and EC_{50} of 2.4 x 10^{-6} M.

(B-C) Effect of a bilateral MBH injection of CCDC or its vehicle on food intake **(B)** and 24h body weight (BW) change **(C)**. 24h fasted DIO mice received 2µg of CCDC (0.2µl per side of 5µg/µL). n=12-15 mice/group.

(D) Daily food intake during chronic icv CCDC (5µg/day) or its vehicle administration in DIO mice. Data correspond to mice in Figure 1I. n=6-7 mice/group.

(E) Area under the curve (AUC) from the insulin tolerance test carried out at the end of the chronic icv treatment in DIO mice fasted 6h.Data correspond to mice in Figure 1M. n=9-16 mice/group.

Data are mean ± SEM. For (B, D), a repeated measures two-way ANOVA was carried out, followed by a Fisher's LSD test. For (C, E), statistics were determined using unpaired t-tests. *p<0.05, ***p<0.001, #p<0.05 treatment effect. See also Table S1.

Figure S2. Metabolic effects of chronic central activation of TGR5 in DIO mice (Related to Figure 2).

(A) Average energy expenditure over 12h at 22°C (dots) or at 30°C (triangles) during chronic icv treatment. Data represent the same days and mice as in Figure 2A. n=6 mice/group.

(B-E) Respiratory exchange ratio (RER, B), mean physical activity (C), and mean meal size (D, E) over 12h at either 22°C (D) or at 30°C (B, C, E). Data represent the same days and mice as in Figure 2A-C. n=6 mice/group.

(F) Plasma levels of total as well as specific BA species measured in blood samples obtained after 10 days of icv infusion of CCDC or its vehicle in free-fed DIO mice. n=8-10 mice/group.

(G) Successful sympathectomy was verified through protein quantification of TH content in the WAT and BAT of DIO mice killed after one week of administration of 6-OH-DOPA (80mg/kg i.p. during 3 consecutive days). Data are presented as the ratio between TH and β-actin per tissue. Representative blots per tissue are depicted to the right of the histogram. n=4 mice/group.

Data are mean ± SEM. For (A), a repeated measures three-way ANOVA was carried out, followed by a Fisher's LSD test. For (B-E) a repeated measures two-way ANOVA was carried out, followed by a Fisher's LSD test. For (F-G), statistics were determined using unpaired t-tests or Mann-Whitney U test. *p<0.05, **p<0.01. See also Table S1.

Figure S3. Characterization of MBH AAV-mediated *TGR5* knockdown (Related to Figure 3).

(A) Representative immunohistological images showing the AAV-Cag-Cre-GFP virus (green) targets mostly neurons (merge between Cre and NeuN panels), but not microglia (merge between Cre and Iba1 panels) or astrocytes (merge between Cre and

GFAP/S100β panels). Top: localization of the AAV within the MBH (3V = third ventricle). Bottom: higher magnification images to highlight cell co-localization, when applicable. Scale bar represents 100 μm in top image and 20 μm in bottom images (applies to all images in a row). Data were obtained from *TGR5^{f/f}*-AAV-Cag-Cre-GFP mice from Figure 3A-E.

(B) DNA gel image showing recombination in hypothalamic brain slices of mice receiving AAV-Cag linked to Cre but not its GFP control, assessed by PCR. Band at 540 bp indicates *TGR5^{f/f}* genotype, whilst the lower thinner band at 390 bp indicates recombination/*TGR5* gene excision. Data correspond to mice from Figure 3A-E. Samples were taken 23 days after AAV injection. Ctrl: control *TGR5^{f/f}* mice receiving AAV-Cag-GFP; Cre: *TGR5^{f/f}* mice receiving AAV-Cag-Cre-GFP; H_2O: negative loading control; WT: C57BL/6J mice as control (band expected at 430 bp); Flox/Flox: positive control for the f/f genotype; +/ex: *TGR5^{f/f}* crossed with a *CMV*-Cre mouse strain as positive control for recombination/gene excision.

(C) mRNA expression of *TGR5* in hypothalamus, cortex, amygdala and VTA of *TGR5^{f/f}* mice receiving AAV-Cag-GFP or AAV-Cag-Cre-GFP. Data correspond to mice from Figure 3 A-E. n=6-8 mice/group.

(D) Daily food intake following the switch to HFD. Data correspond to mice from Figure 3 A-E. n=6-8 mice/group.

(E) Daily food intake following AAV injection in already obese *TGR5^{f/f}* mice. Data correspond to mice from Figure 3F-J. n=9-10 mice/group.

(F) Above: scheme of the knock-in construct of the *TGR5-Tdt* reporter mouse model. Beige bar, *TGR5* exon; an Hemagglutin (HA) Tag was inserted 3' in frame with the unique TGR5 exon after stop codon removal in order to generate a tagged TGR5

protein, a tandem Tomato (Tdt) Tag was inserted downstream an IRES sequence in order to use Tdt expression as a surrogate marker for TGR5 expression. Below: mRNA expression of *TGR5*, *hemagglutinin* and *tandem Tomato* in ileum and colon of control wild-type (WT) and *TGR5-Tdt* mice. n=2 WT and 4 *TGR5-Tdt* mice.

(G) Representative images of the targeted cells in the MBH (3V= third ventricle) of *VGAT*-ires-Cre (left) and of *vGlut2*-ires-Cre (right) mice having received an intrahypothalamic administration of pAAV-hSyn-DIO-mCherry showing expected location for GABAergic and glutamatergic cells, respectively (scale bar: 100 μm). Inserts illustrate the single cell laser capture microdissection (before on the left and after on the right; scale bar: 10 μm).

(H) mRNA expression of *TGR5*, *VGAT* and *vGlut2* in fluorescent laser capture microdissected cells obtained from the MBH of *VGAT*-ires-Cre and of *vGlut2*-ires-Cre mice having received an intrahypothalamic administration of pAAV-hSyn-DIO-mCherry to label GABAergic or glutamatergic cells, respectively. n=3-4 mice/group.

Data are mean ± SEM. For (C), an unpaired t-test was performed using ΔCT values; data are represented as fold change from the *TGR5^{f/f}*-AAV-Cag-GFP group. For (D-E), a repeated measures two-way ANOVA was carried out, followed by a Fisher's LSD test. For (D) $*p<0.05$ or $**p<0.01$ between *TGR5^{f/f}*-AAV-Cag-Cre-GFP compared to *TGR5^{f/f}*-AAV-Cag-GFP group; $\$p<0.01$ between C57BL/6J and both *TGR5^{f/f}* groups. For (F, H) no statistical analysis was carried out due to the low n of samples. For (F), data are expressed as fold change from the WT group, for (H) data are represented as fold change from the *VGAT*-ires-Cre group. $*p<0.05$. $\#p<0.05$ treatment effect. See also Table S1.

Figure S4. Impact of astrocytic MBH *TGR5* knockdown on energy balance (Related to Figure 3).

(A) Representative immunohistological images showing the AAV-GFAP-Cre-mCherry (red) targets mostly astrocytes (merge between Cre and GFAP/S100β panels), but not neurons (merge between Cre and NeuN panels) or microglia (merge between Cre and Iba1 panels). Top: localization of the AAV within the MBH (3V= third ventricle). Bottom: higher magnification images to highlight cell co-localization, when applicable. Scale bar represents 100 μm in top image and 20 μm in bottom images (applies to all images in a row).

(B) DNA gel image showing recombination in hypothalamic brain slices of mice receiving AAV-GFAP linked to Cre or their controls, assessed by PCR. Band at 540 bp indicates *TGR5*^*f/f* genotype, whilst the lower thinner band at 390 bp indicates recombination/*TGR5* gene excision. Data represent the same mice as in Figure 3 N-R. Samples were taken ~25 days after AAV injection. Ctrl: control *TGR5*^*f/f* mice receiving AAV-GFAP-mCherry; Cre: *TGR5*^*f/f* mice receiving AAV-GFAP-Cre-mCherry; H_2O: negative loading control; WT: C57BL/6J mice as control (band expected at 430 bp); Flox/Flox: positive control for the f/f genotype; +/ex: *TGR5*^*f/f* crossed with a CMV-Cre mouse strain as positive control for recombination/gene excision.

(C) Hypothalamic mRNA expression of *TGR5* in *TGR5*^*f/f* mice receiving AAV-GFAP-mCherry or AAV-GFAP-Cre-mCherry. Samples were taken 25 days post AAV injection. n=7 mice/group.

(D-H) BW **(D)**, body composition **(E-F)**, cumulative food intake **(G)** and feed efficiency **(H)** following bilateral AAV-GFAP-mCherry control injection or AAV-GFAP-Cre-mCherry

mediated knockdown of astrocytic *TGR5* in the MBH in *TGR5^{f/f}* mice. Animals were on chow and then switched to a HFD (arrow). n=7-8 mice/group.

Data are mean ± SEM. For (C), an unpaired t-test was performed using ΔCT values; data are represented as fold change from the *TGR5^{f/f}*-AAV-GFAP-mCherry group. For (D), a repeated measures two-way ANOVA was carried out, followed by a Fisher's LSD test. For (E-H), an unpaired t-test was performed.

*p<0.05. See also Table S1.

Figure S5. Role of hypothalamic TGR5 in the anti-obesity action of BA supplementation (Related to Figure 4).

(A-E) Daily food intake (**A**), cumulative food intake (**B**), BW gain (**C**), fat mass gain (**D**), and feed efficiency (**E**) of *TGR5^{f/f}* mice with (Cre) or without (GFP) hypothalamic knockdown of *TGR5*, and exposed to either a HFD or a HFD enriched with 0.5% CA. Data correspond to mice from Figure 4 A-E. n=8-10 mice/group.

(F) Food preference test in naïve *TGR5^{f/f}* lean chow-fed mice. Animals preferred eating the HFD enriched with 0.5% CA rather than standard chow diet when having the choice over 1h. n=5 mice/group.

Data are mean ± SEM. For (A), a repeated measures three-way ANOVA was carried out, followed by a Fisher's LSD test. For (B-E), a two-way ANOVA was carried out, followed by a Fisher's LSD test. For (F), an unpaired t-test was carried out. $^{\$\$\$}$p<0.001 effect of CA supplementation; $^{\#\#\#}$p<0.001 effect of TGR5 knockdown. ***p<0.001. See also Table S1.

Table S2. Mean ± SEM values of plasma and hypothalamic BA species in chow-fed and DIO mice (Related to Figure 1).

BA species		Plasma (nM)	Hypothalamus (fmol/mg tissue)
Total BA	Chow	1735.16 ± 441.07	28.86 ± 3.70
	DIO	1123.84 ± 153.88	16.79 ± 2.45
CA	Chow	67.51 ± 26.04	1.08 ± 0.47
	DIO	60.19 ± 27.52	1.05 ± 0.63
DCA	Chow	135.57 ± 27.35	4.69 ± 0.60
	DIO	75.14 ± 15.75	2.10 ± 0.45
CDCA	Chow	8.06 ± 3.94	1.04 ± 0.19
	DIO	7.10 ± 4.77	0.80 ± 0.12
UDCA	Chow	11.50 ± 4.25	N.D.
	DIO	6.79 ± 2.18	N.D.
LCA	Chow	5.19 ± 0.99	N.D.
	DIO	6.66 ± 1.32	N.D.
αMCA	Chow	5.92 ± 2.36	0.99 ± 0.49
	DIO	6.45 ± 1.20	0.92 ± 0.32
βMCA	Chow	47.86 ± 14.79	0.74 ± 0.31
	DIO	14.93 ± 3.29	N.D.
ωMCA	Chow	73.82 ± 13.99	1 ± 0.32
	DIO	65.42 ± 11.73	0.51 ± 0.13
HDCA	Chow	13.22 ± 2.92	N.D.
	DIO	10.06 ± 2.62	N.D.
TCA	Chow	608.04 ± 185.46	9.92 ± 1.60
	DIO	349.57 ± 81.05	5.19 ± 0.75
TDCA	Chow	125.11 ± 18.56	1.65 ± 0.17
	DIO	69.08 ± 15.40	1 ± 0.25
TCDCA	Chow	19.38 ± 2.63	0.22 ± 0.03
	DIO	23.95 ± 3.79	0.40 ± 0.05

TUDCA	Chow	11.82 ± 1.40	0.25 ± 0.03
	DIO	33.71 ± 3.98	0.35 ± 0.06
TLCA	Chow	0.83 ± 0.08	N.D.
	DIO	0.81 ± 0.13	N.D.
GCA	Chow	4.06 ± 0.65	N.D.
	DIO	0.80 ± 0.29	N.D.
TαMCA	Chow	107.5 ± 35.12	1.34 ± 0.20
	DIO	83.61 ± 16.28	1.04 ± 0.18
TβMCA	Chow	261.31 ± 112.88	4.30 ± 1.38
	DIO	91.02 ± 15.18	1.38 ± 0.34
TωMCA	Chow	229.34 ± 40.82	3.02 ± 0.52
	DIO	218.56 ± 21.58	2.53 ± 0.30

Table S3. Pharmacokinetics of the CCDC compound (Related to Figure 1).
Assessment of CCDC concentrations (nM) by liquid-chromatography-mass spectrometry in the plasma, hypothalamus and rest of the brain of DIO mice receiving acute icv CCDC (5µg) and in the plasma of DIO mice receiving chronic icv CCDC treatment (5µg/day). In preliminary studies, we found that the EC_{50} of CCDC on mouse TGR5 is of 91nM. N/A: not analyzed.

		[CCDC] sample (nM)		
	Time	**Plasma**	**Hypothalamus***	**Rest of the brain***
Acute	15 min	22 18 < 3	9671 4710 14	3651 1957 8
	30 min	< 3 < 3 < 3	13 7 < 5	160 883 287
	60 min	< 3 < 3 < 3	< 5 < 5 15	11 49 2274
	120 min	< 3 < 3 < 3	24 24 6	31 26 12
	240 min	< 3 < 3 < 3	7 < 5 < 5	21 7 8
Chronic	At 28 days	< 3 < 3 < 3	N/A N/A N/A	N/A N/A N/A

1 gr of tissue is assimilated to 1mL of tissue

Table S4. qPCR primers for several tissues and cells (Related to STAR Methods).

Gene name	Tissue	GenBank ID	Forward primer	Reverse primer
Adrb1	WAT, BAT	NM_007419	TTCTCCTAGAGGGCAAACCTTGT	CAGAGTGAGGTAGAGGACCCACA
Adrb2	WAT, BAT	NM_007420	CTGTGCCTTCGCAGGTCTTC	TCCGTTCTGCCGTTGCTATT
Adrb3	WAT, BAT	NM_013462	CGACATGTTCCTCCACAAATCA	TGGATTCCTGCTCTCAAACTAACC
Bsep (Abcb11)	Hypothalamus	NM_021022	ACTTGGTGACAGAGAGCATGGA	AAGGAGCTTTCCCAAATGCA
Cidea	WAT	NM_007702	TTCAAGGCCGTGTTAAGGAATC	CCAGGAACTGTCCCGTCATC
Dio2	WAT, BAT	NM_010050	CAGACTCACCAGCCCATGTAAC	CGCACACCAGTGAGCTCTGA
Eef1a1	Hypothalamus; Microdissected cells	NM_010106	CCATGTGTGTTGAGAGCTTTC	GCAACTGTCTGCCTCATGTCA
Gapdh	Several tissues; Microdissected cells	NM_008084	TCAAGAAGGTGGTGAAGCAG	TGGGAGTTGCTGTTGAAGTC
HA-Tag	Ileum, colon		ACCACACCAGTAGCCAATGC	AAGCGTAATCTGGAACATCG
Hsl (Lipe)	WAT	NM_010719	GGGAGTGGGCTGTGCCTTA	TCCCCCAGGTTCAGCTTTT
Insr	WAT	NM_010568	GAAAAACCTTCCAGTATGTTCCTCA	TGTTATTCCCATTGCCCAACTT
Nono	WAT, BAT	NM_023144	CTGTCTGGTGCATTCCTGAACTAT	AGCTCTGAGTTCATTTTCCCATG
Ntcp (Slc10a1)	Liver	NM_001177561	AAACCTTCAACAGCAGAATCATGA	GGATGATGGTTCCTGGATAGATG
Ostα (Slc51a)	Liver	NM_145932	TTGGACCCTGGAAGACATACTGTA	CTGATAAGGCTGAGGGACAGAAG
Pgc1α	WAT, BAT	AF049330	CAACCATACCAGAACAAGAACAA	AAGCTGACACCCGTGAATAAAC
Pparα	WAT	NM_001113418	GGCACATTTCCAAAGCAAGG	AGGATGGCACCAAGGACAGTA
Ppia	Several tissues	NM_008907	CAAATGCTGGACCAAACACAA	GCCATCCAGCCATTCAGTCT
Ppia	Ileum, colon	NM_008907	GCATACGGGTCCTGGCATCTTGTCC	ATGGTGATCTTCTTGCTGGTCTTGC
Prdm16	WAT	NM_027504	GAAAAAAAAATGGACCACAGTTCC	CGTCTTCTCGATTCACGATTCTCT
Rpl13a	Hypothalamus	NM_009438	CGCCGCCAACTAGGGAA	GGTGCGCTGTCAGCTCTCTAAT
Sdha	Several tissues	NM_023281	TACAAAGTGCGGGTCGATGA	TGTTCCCCAAACGGCTTCT
Slc2a4	WAT	NM_001042	TCGAGTGCAGTGGCGTGAT	GCTGAGGCAGGAGAATGGC
Tandem Tomato	Ileum, colon		GGCAGATATCCCGGACTACA	AGCGATGAATCTTGGGTCAC
TGR5 (Gpbar1)	Different brain structures; Microdissected cells	NM_174985	CCTTTCCCTGCTTGCCAAT	CCGGAGTGGCTGCAACAC
TGR5 (Gpbar1)	Ileum, colon	NM_174985	CTACTGGTCCTGCCTCCTTCTC	AACACTGCCATGTAGCGTTCC
Trib3	WAT	NM_175093	TTGGGCCAAGCTAAACCTTAAGT	GCACAGGAACGAATAAGGCAC
Tuba4a	Hypothalamus	NM_009447	CTGGACCACAAGTTTGACTTGATG	TCCATTCCCTCACCCACATAC

VGAT(Slc32a1)	Microdissected cells	NM_009508	GCGGGCTGGAACGTGACAA	GTGGAGGATGGCGTAGGGTA
vGlut2 (Slc17a6)	Microdissected cells	NM_080853	CATTGTTGGTGCAATGACAAAG	GTGCAGCAATGAGGAAGACAT
Ywhaz	Hypothalamus	NM_011740	CTTGTGAGGCTGTGACACAAACA	CAAGAGTGTGCACGCAGACA

TaqMan®Probe used for qPCR on FACS-isolated hypothalamic cells

Gene name	GenBank ID	TaqMan®Probe
Actb	NM_007393.5	Mm00607939_s1
Bdnf	NM_007540.4	Mm01334047_m1
GAD1	NM_008077.4	Mm04207432_g1
GAD2	NM_008078.2	Mm00484623_m1
Lepr	NM_001122899.1	Mm00440181_m1
Npy	NM_023456.2	Mm01410146_m1
Pomc	NM_001278581.1	Mm00435874_m1
SF1	NM_139051	Mm00496060_m1
Sim1	NM_011376.3	Mm00441390_m1
vGlut2 (Slc17a6)	NM_080853.3	Mm00499876_m1
vGlut1 (Slc17a7)	NM_182993.2	Mm00812886_m1
VGAT (Slc32a1)	NM_009508.2	Mm00494138_m1
Th	NM_009377.1	Mm00447557_m1
TGR5 (Gpbar1)	NM_174985.1	Mm04212121_s1
Trh	NM_009426.3	Mm01182425_g1
Rn18s	NR_003278.3	Mm03928990_g1

Figure S1

A

TGR5

- BA mix
- LCA

Luciferase (%) vs log (M)

B

Food intake (g) vs Time (hours)

- DIO/Vehicle
- DIO/CCDC

***

C

24h BW change (g)

*

D

Food intake (g) vs Days of icv treatment

- DIO/Vehicle
- DIO/CCDC

#

E

AUC

*
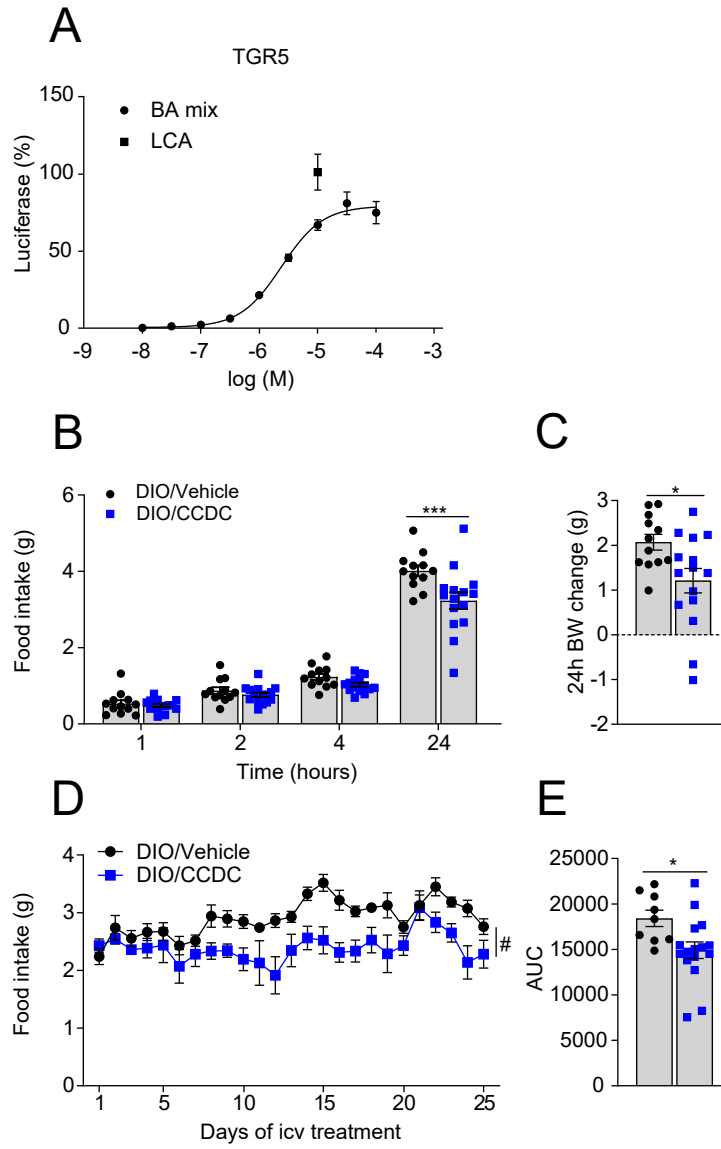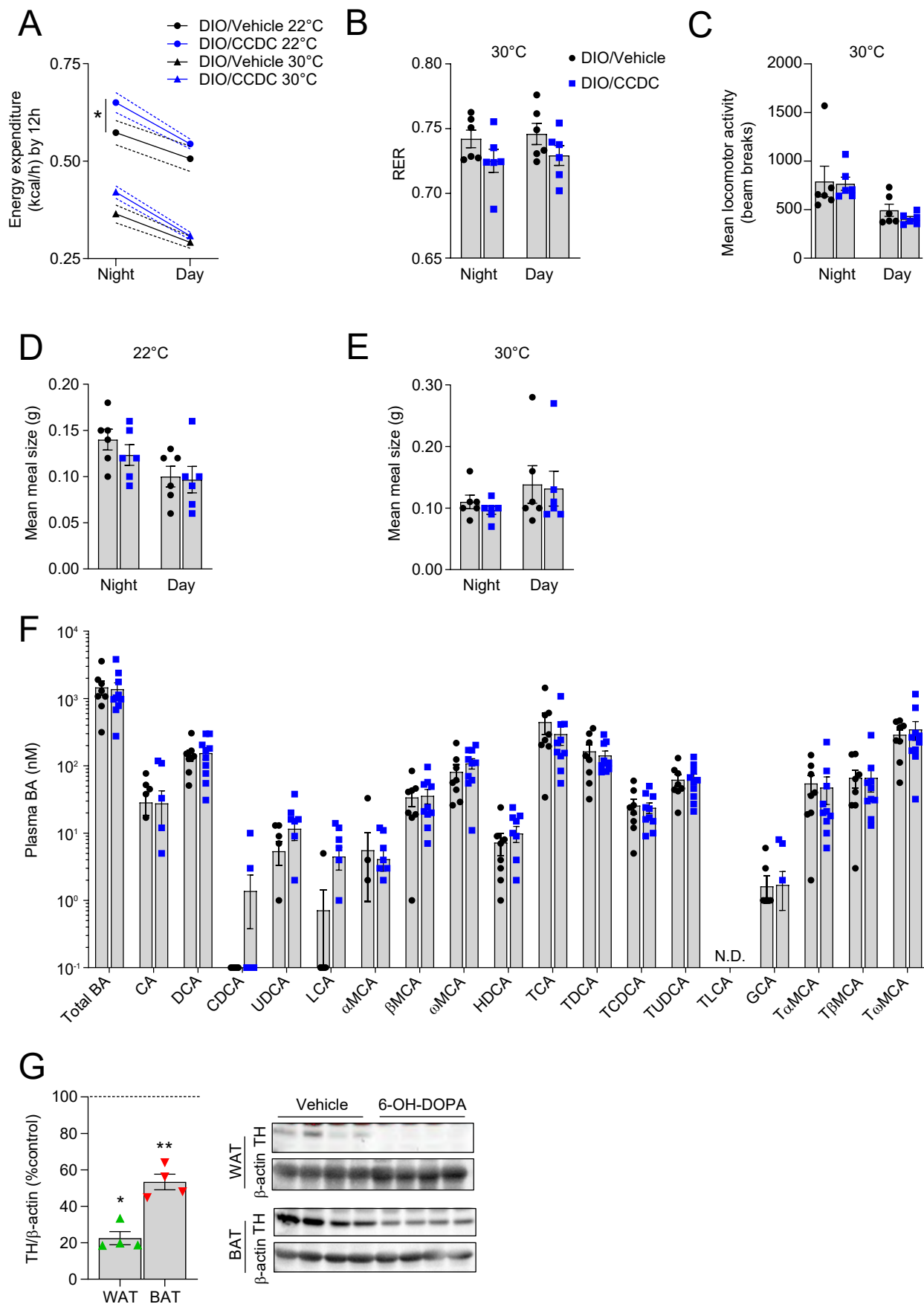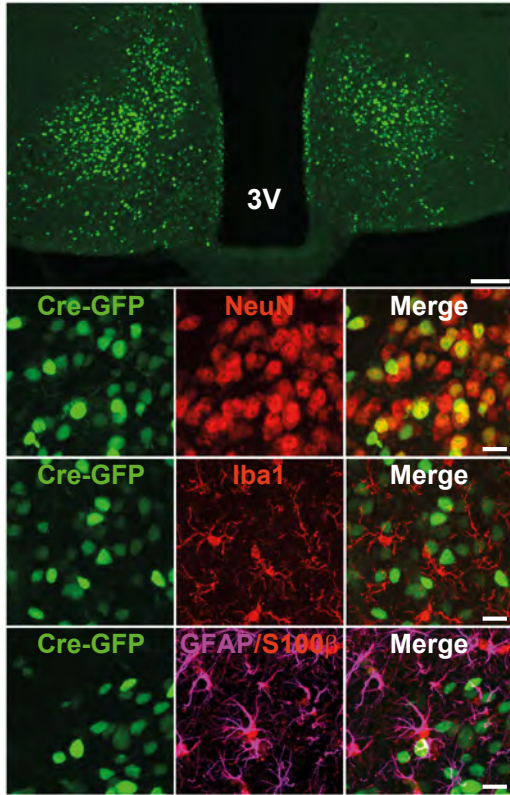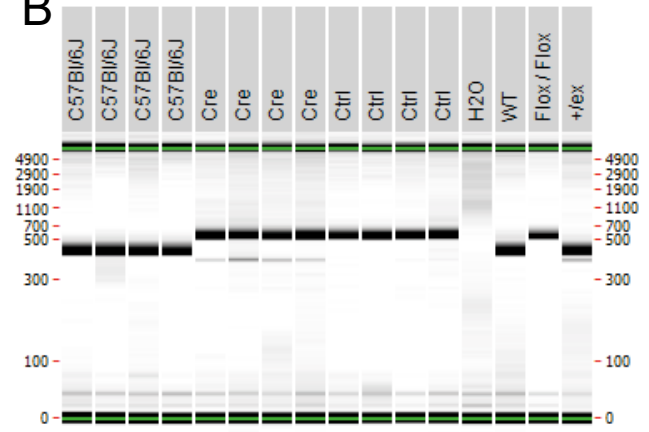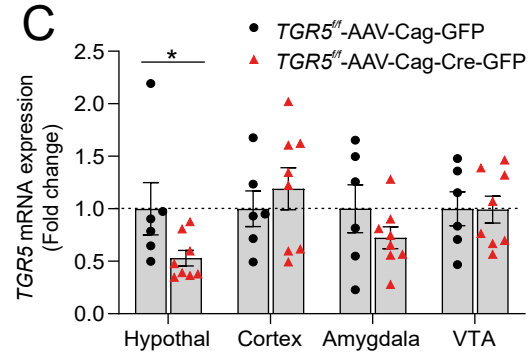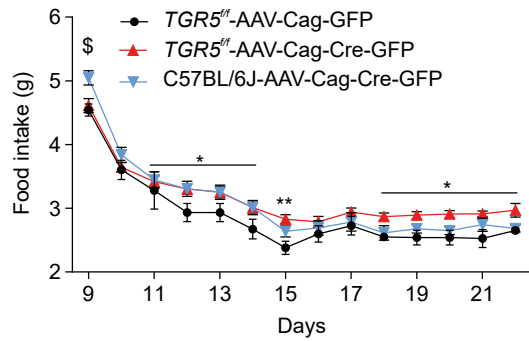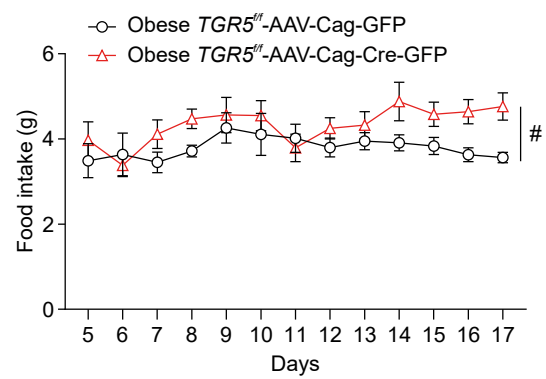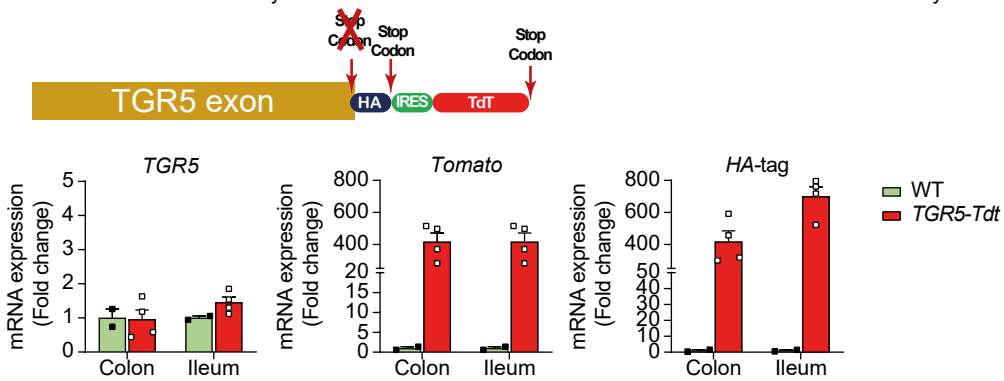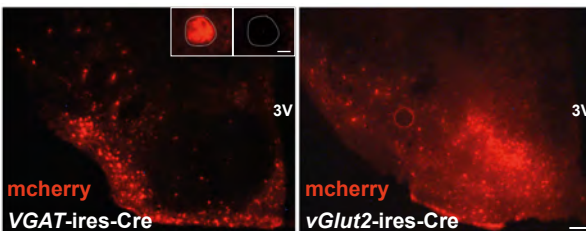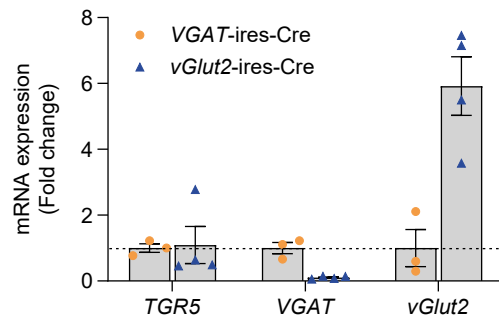
Figure S2
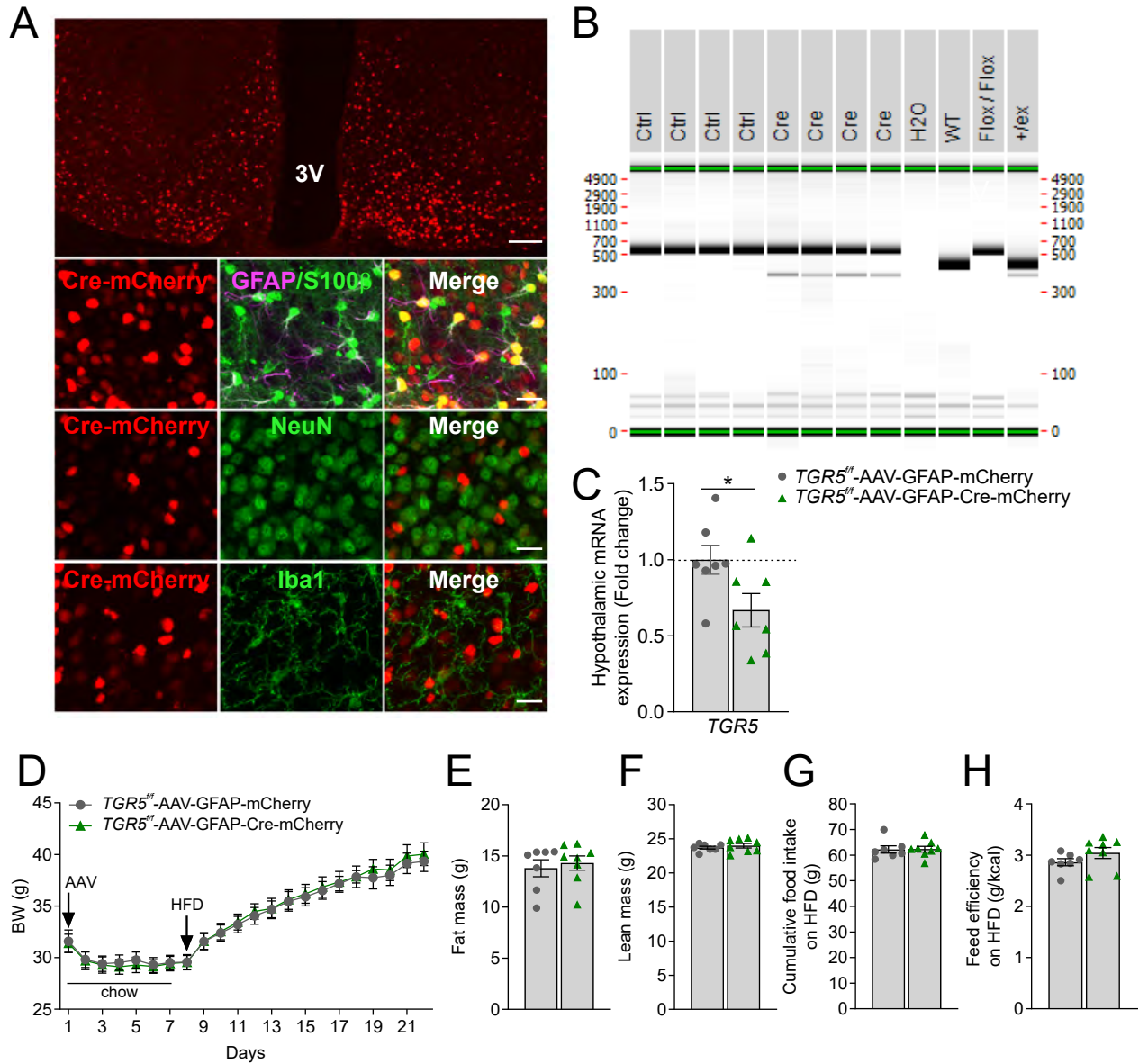
Figure S3

Figure S4

Figure S5
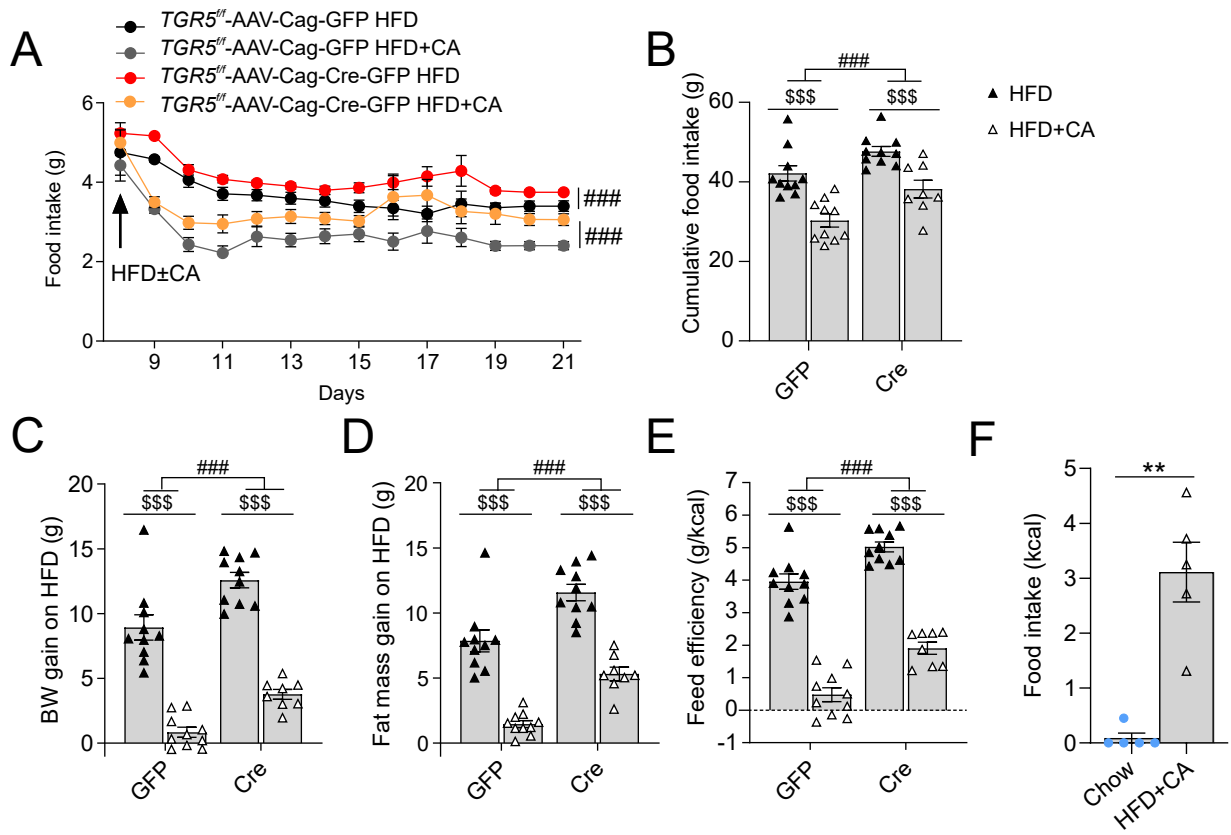
Highlights

- Diet-induced obesity induces changes in the hypothalamic BA-TGR5 system

- Central TGR5 agonism reduces obesity by activating the sympathetic nervous system

- Hypothalamic TGR5 protects from the onset and worsening of diet-induced obesity

- Hypothalamic TGR5 participates to the anti-obesity effects of BA supplementation

eTOC Blurb

Castellanos-Jankiewicz et al. demonstrate that activation of central TGR5 signaling counteracts diet-induced obesity, whereas genetic downregulation of hypothalamic TGR5 promotes it. These effects involve modulation of food intake and of energy expenditure through the sympathetic nervous system, revealing a long-range bile acids-dependent hypothalamic mechanism contributing to weight regulation in obesity.

Diet-Induced Obesity

Hypothalamic TGR5

SUPPRESSION

STIMULATION

SNS

↑ Body Weight ↓
↑ Food Intake ↓
↑ Fat Mass ↓
↓ Energy Expenditure ↑

Table S1. Statistical analyses for main and supplementary figures (Related to STAR Methods)

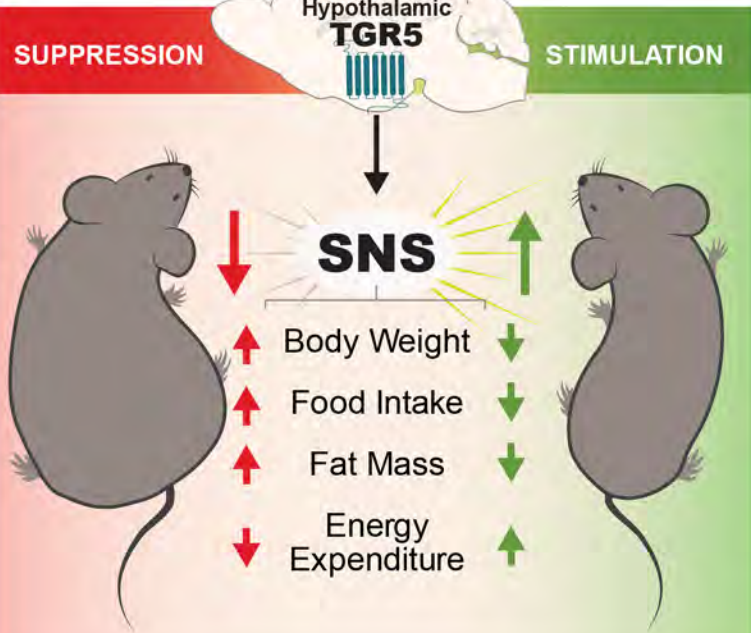| Figure	Dependent variable(s)	Factor Analyzed	Analysis	n	Degree of freedom & F/t/R etc value	P value
1A	Plasma BA	Diet	Unpaired t-test or Mann Whitney U test; two tailed	Chow=8-9 HFD=8	**Total BA** U:21 **CA** t(15)=0.1934 **DCA** t(15)=1.851 **CDCA** t(14)=0.1513 **UDCA** t(15)=0.9494 **LCA** t(15)=0.9028 **αMCA** t(15)=0.1900 **βMCA** U:19 **ωMCA** t(15)=0.4533 **HDCA** t(15)=0.7992 **TCA** U: 20 **TDCA** t(15)=2.288 **TCDCA** t(15)=1.011 **TUDCA** U:0 **TLCA** t(15)=0.0855 **GCA** U:3 **TαMCA** U:30 **TβMCA** U:13 **TωMCA** t(15)=0.2249	**Total BA** p=0.1672 **CA** p=0.8493 **DCA** p=0.0840 **CDCA** p=0.8819 **UDCA** p=0.3575 **LCA** p=0.3809 **αMCA** p=0.8519 **βMCA** p=0.1139 **ωMCA** p=0.6568 **HDCA** p=0.4366 **TCA** p=0.1388 **TDCA** p=0.0370 **TCDCA** p=0.3280 **TUDCA** p<0.0001 **TLCA** p=0.9329 **GCA** p=0.0005 **TαMCA** p=0.6058 **TβMCA** p=0.0274 **TωMCA** p=0.8251
1B	Hypothal BA	Diet	Unpaired t-test or Mann Whitney U test; two tailed	Chow=4-9 HFD=4-8	**Total BA** t(15)=2.645 **CA** t(8)=0.03135 **DCA** t(15)=3.360 **CDCA** t(12)=1.091 **UDCA** N.D. **LCA** N.D. **αMCA** t(13)=0.1249 **βMCA** no stat due to undetectable levels in DIO **ωMCA** t(12)=1.419 **HDCA** N.D. **TCA** U: 9 **TDCA** t(15)=2.210 **TCDCA** t(13)=2.905 **TUDCA** t(10)=1.236 **TLCA** N.D. **GCA** N.D. **TαMCA** t(15)=1.108 **TβMCA** U:9 **TωMCA** t(15)=0.7939	**Total BA** p=0.0184 **CA** p=0.9758 **DCA** p=0.0043 **CDCA** p=0.2967 **UDCA** N.D. **LCA** N.D. **αMCA** p=0.9025 **βMCA** no stat due to undetectable levels in DIO **ωMCA** p=0.1812 **HDCA** N.D. **TCA** p=0.0079 **TDCA** p=0.0431 **TCDCA** p=0.0123 **TUDCA** p=0.2446 **TLCA** N.D. **GCA** N.D. **TαMCA** p=0.2852 **TβMCA** p=0.0079 **TωMCA** p=0.4396
1D	deltaCT	Feeding condition	Unpaired t-test; two tailed	**Chow** fasted=6 fed=5 **HFD** fasted=7 fed=7	**Chow** **Ostα** t(9)=1.795 **Ntcp** t(9)=1.628 **Bsep** t(9)=3.130 **TGR5** t(9)=2.334 **HFD** **Ostα** t(12)=0.4647 **Ntcp** t(12)=0.011 **Bsep** t(12)=0.2443 **TGR5** t(12)=0.7903	**Chow** **Ostα** p=0.112 **Ntcp** p=0.137 **Bsep** p=0.0121 **TGR5** p=0.044 **HFD** **Ostα** p=0.6504 **Ntcp** p=0.9914 **Bsep** p=0.8111 **TGR5** p=0.4447
1E	Food intake	Time & Treatment	RM Two-way ANOVA	Vehicle=6 CCDC 2.5µg=9 CCDC 5µg=9	Time: F(3,63)=226.0 Treatment: F(2,21)=3.984 Interaction: F(6,63)=2.488	Time: p<0.0001 Treatment: p=0.0341 Interaction: p=0.0318
1F	Body weight change	Treatment	One-way ANOVA	Vehicle=6 CCDC 2.5µg=9 CCDC 5µg=9	F(2,21)=6.040	p=0.0085
1G	Food intake	Time & Treatment	RM Two-way ANOVA	Vehicle=10 BA mix 5µg=12	Time: F(3,60)=383.9 Treatment: F(1,20)=1.885 Interaction: F(3,60)=6.198	Time: p<0.0001 Treatment: p=0.1849 Interaction: p=0.0010
1H	Body weight change	Treatment	Unpaired t-test; two tailed	Vehicle=10 BA mix 5µg=12	t(20)=2.234	p=0.0371
					Time: F(24,264)=2.861	Time: p<0.0001

1I	Body weight	Time & Treatment	RM Two-way ANOVA	Vehicle=6 CCDC=7	Treatment: $F_{(1,11)}=6.858$ Interaction: $F_{(24,264)}=14.02$	Treatment: p=0.0239 Interaction: p<0.0001
1J	Fat mass	Treatment	Unpaired t-test; two tailed	Vehicle=6 CCDC=7	$t_{(11)}=4.280$	p=0.0013
1K	Lean mass	Treatment	Unpaired t-test; two tailed	Vehicle=6 CCDC=7	$t_{(11)}=0.4301$	p=0.6754
1L	Cumulative food intake	Treatment	Unpaired t-test; two tailed	Vehicle=6 CCDC=7	$t_{(11)}=4.172$	p=0.0016
1M	Glycemia	Time & Treatment	RM Two-way ANOVA	Vehicle=9 CCDC=16	Time: $F_{(5,115)}=50.10$ Treatment: $F_{(1,23)}=5.853$ Interaction: $F_{(5,115)}=2.588$	Time: p<0.0001 Treatment: p=0.0239 Interaction: p=0.0295
1N	Feed efficiency	Treatment	Unpaired t-test; two tailed	Vehicle=6 CCDC=7	$t_{(11)}=4.379$	p=0.0011
2A	Energy expenditure	Time & Treatment	RM Two-way ANOVA	6 per group	**22°C:** Time: $F_{(23,230)}=14.49$ Treatment: $F_{(1,10)}=2.466$ Interaction: $F_{(23,230)}=1.875$ **30°C:** Time: $F_{(23,230)}=22.31$ Treatment: $F_{(1,10)}=2.61$ Interaction: $F_{(23,230)}=1.413$	**22°C:** Time: p<0.0001 Treatment: p=0.1474 Interaction: p=0.0109 **30°C:** Time: p<0.0001 Treatment: p=0.1373 Interaction: p=0.1051
2B	RER	Time and treatment	RM Two-way ANOVA	6 per group	Time: $F_{(1, 10)} = 85.59$ Treatment: $F_{(1, 10)} = 4.338$ Interaction: $F_{(1, 10)} = 2.497$	Time: p<0.0001 Treatment: p=0.0639 Interaction: p=0.1451
2C	Locomotor activity	Time and treatment	RM Two-way ANOVA	6 per group	Time: $F_{(1,10)} = 30.91$ Treatment: $F_{(1,10)} = 4.042$ Interaction: $F_{(1,10)} = 0.2149$	Time: p=0.0002 Treatment: p=0.0721 Interaction: p=0.6529
2D	deltaCT	Treatment	Unpaired t-test; two tailed	Vehicle=5-6 CCDC=7	β1-AR: $t_{(11)}=2.563$ β2-AR: $t_{(11)}=2.783$ β3-AR: $t_{(11)}=3.057$ Hsl: $t_{(11)}=0.6511$ Dio-2: $t_{(10)}=0.6686$	β1-AR: p=0.0264 β2-AR: p=0.0178 β3-AR: p=0.0109 Hsl: p=0.5284 Dio-2: p=0.5189
2E	deltaCT	Treatment	Unpaired t-test; two tailed	Vehicle=6 CCDC=7	β1-AR: $t_{(11)}=0.8530$ β2-AR: $t_{(11)}=3.583$ β3-AR: $t_{(11)}=1.421$ Pgc1α: $t_{(11)}=1.127$ Dio-2: $t_{(11)}=2.202$	β1-AR: p=0.4118 β2-AR: p=0.0043 β3-AR: p=0.1830 Pgc1α: p=0.2838 Dio-2: p=0.0499
2F	deltaCT	Treatment	Unpaired t-test or Mann Whitney U test; two tailed	Vehicle=12 CCDC=10	β1-AR: $t_{(20)}=0.3327$ β2-AR: $t_{(20)}=0.3633$ β3-AR: $t_{(20)}=0.3600$ Hsl: $t_{(20)}=0.2748$ Dio-2: $t_{(20)}=0.3358$	β1-AR: p=0.7428 β2-AR: p=0.7202 β3-AR: p=0.7226 Hsl: p=0.7863 Dio-2: p=0.7405
2G	deltaCT	Treatment	Unpaired t-test or Mann Whitney U test; two tailed	Vehicle=12 CCDC=10	β1-AR: $t_{(20)}=0.4698$ β2-AR: $t_{(20)}=0.0238$ β3-AR: $t_{(20)}=0.0640$ Pgc1α: U=59 Dio-2: $t_{(20)}=0.6715$	β1-AR: p=0.6436 β2-AR: p=0.9812 β3-AR: p=0.9495 Pgc1α: p=0.9742 Dio-2: p=0.5096
2H	Body weight	Time & Treatment	RM Two-way ANOVA	9 per group	Time: $F_{(24,384)}=121.7$ Treatment: $F_{(1,16)}=2.881$ Interaction: $F_{(24,384)}=2.831$	Time: p<0.0001 Treatment: p=0.1090 Interaction: p<0.0001
2I	Fat mass	Treatment	Unpaired t-test; two tailed	9 per group	$t_{(16)}=1.998$	p=0.0630
2J	Lean mass	Treatment	Unpaired t-test; two tailed	9 per group	$t_{(16)}=0.0253$	p=0.9801
2K	Cumulative food intake	Treatment	Unpaired t-test; two tailed	9 per group	$t_{(16)}=2.041$	p=0.0581
3A	Body weight	Time & Genotype	RM Two-way ANOVA	*TGR5^{f/f}*-AAV-Cag-GFP=6 *TGR5f/f-AAV-Cag-Cre-GFP=8 C57BL/6J-AAV-Cag-Cre-GFP=8*	Time: $F_{(21,399)}=217.9$ Genotype: $F_{(2,19)}=2.223$	Time: p<0.0001 Genotype: p=0.1357

				Interaction: F(42,399)=6.130	Interaction: p<0.0001
3B	Fat mass	Genotype	One-way ANOVA	*TGR5ʰ/ʰ-AAV-Cag-GFP=6* *TGR5f/f-AAV-Cag-Cre-GFP=8* *C57BL/6J-AAV-Cag-Cre-GFP=8*	F(2,19)=5.421	p=0.0137
3C	Lean mass	Genotype	One-way ANOVA	*TGR5ʰ/ʰ-AAV-Cag-GFP=6* *TGR5f/f-AAV-Cag-Cre-GFP=8* *C57BL/6J-AAV-Cag-Cre-GFP=8*	F(2,19)=0.649	p=0.5338
3D	Cumulative food intake	Genotype	One-way ANOVA	*TGR5ʰ/ʰ-AAV-Cag-GFP=6* *TGR5f/f-AAV-Cag-Cre-GFP=8* *C57BL/6J-AAV-Cag-Cre-GFP=7*	F(2,18)=4.301	p=0.0297
3E	Feed efficiency	Genotype	One-way ANOVA	*TGR5f/f-AAV-Cag-GFP=6* *TGR5f/f-AAV-Cag-Cre-GFP=8* *C57BL/6J-AAV-Cag-Cre-GFP=7*	F(2,18)=6.26	p=0.0086
3F	Body weight	Time & Genotype	RM Two-way ANOVA	10 per group	Time: F(16,288)=307.2 Genotype: F(1,18)=0.7483 Interaction: F(16,288)=17.95	Time: p<0.0001 Genotype: p=0.3984 Interaction: p<0.0001
3G	Fat mass	Genotype	Unpaired t-test; two tailed	*TGR5ʰ/ʰ-AAV-Cag-GFP=10* *TGR5f/f-AAV-Cag-Cre-GFP=9*	t(17)=2.585	p=0.0193
3H	Lean mass	Genotype	Unpaired t-test; two tailed	*TGR5ʰ/ʰ-AAV-Cag-GFP=10* *TGR5f/f-AAV-Cag-Cre-GFP=9*	t(17)=0.9039	p=0.3787
3I	Cumulative food intake	Genotype	Unpaired t-test; two tailed	*TGR5ʰ/ʰ-AAV-Cag-GFP=9* *TGR5f/f-AAV-Cag-Cre-GFP=10*	t(17)=2.349	p=0.0312
3J	Feed efficiency	Genotype	Unpaired t-test; two tailed	*TGR5ʰ/ʰ-AAV-Cag-GFP=9* *TGR5f/f-AAV-Cag-Cre-GFP=10*	t(17)=3.957	p=0.0010
3K	Ratio	Genotype	Unpaired t-test; two tailed	*TGR5ʰ/ʰ-AAV-Cag-GFP=7* *TGR5f/f-AAV-Cag-Cre-GFP=6*	t(11)=3.553	p=0.0045
3L	Ratio	Genotype	Unpaired t-test; two tailed	*TGR5ʰ/ʰ-AAV-Cag-GFP=7* *TGR5f/f-AAV-Cag-Cre-GFP=6*	t(11)=2.269	p=0.0444
3M	deltaCT	Genotype	Unpaired t-test or Mann Whitney *U* test; one tailed	*TGR5ʰ/ʰ-AAV-Cag-GFP=7* *TGR5f/f-AAV-Cag-Cre-GFP=6*	β1-AR: t(11)=0.353 β2-AR: t(11)=1.099 β3-AR: t(11)=1.915 Hsl: t(11)=2.056 Insr: U=8 Trib3: t(11)=1.513 Slc2a4: U=8 Cidea: U=10 Prdm16: t(11)=0.0226 Pgc1α: t(11)=0.4074 Pparα: t(11)=2.633	β1-AR: p=0.3652 β2-AR: p=0.1476 β3-AR: p=0.0409 Hsl: p=0.0321 Insr: p=0.0367 Trib3: p=0.0793 Slc2a4: p=0.0367 Cidea: p=0.0688 Prdm16: p=0.4912 Pgc1α: p=0.3458 Pparα: p=0.0116
3N	Body weight	Time & Genotype	RM Two-way ANOVA	*TGR5ʰ/ʰ-AAV-Cag-GFP=10* *TGR5f/f-AAV-Cag-Cre-GFP=10*	Time: F(1.946,35.02) = 246.2 Genotype: F(1,18) = 0.02985 Interaction: F(28,504) = 1.303	Time: P<0.0001 Genotype: P=0.8648 Interaction: P=0.1394
3O	Fat mass	Genotype	Unpaired t-test; two tailed	*TGR5ʰ/ʰ-AAV-Cag-GFP=10* *TGR5f/f-AAV-Cag-Cre-GFP=10*	t(18)=0.9382	p=0.3606

3P	Lean mass	Genotype	Unpaired t-test; two tailed	*TGR5^f/f* -AAV-Cag-GFP=10 *TGR5f/f-AAV-Cag-Cre-GFP=10*	t(18)=0.6985	p=0.4938
3Q	Cumulative food intake	Genotype	Unpaired t-test; two tailed	*TGR5^f/f* -AAV-Cag-GFP=9 *TGR5f/f-AAV-Cag-Cre-GFP=10*	t(17)=0.5173	p=0.6116
3R	Feed efficiency	Genotype	Unpaired t-test; two tailed	*TGR5^f/f* -AAV-Cag-GFP=9 *TGR5f/f-AAV-Cag-Cre-GFP=10*	t(17)=1.829	p=0.0850
4A	Body weight	Time, Genotype & Diet	RM Three-way ANOVA	*TGR5^f/f* -AAV-Cag-GFP HFD=10 *TGR5f/f-AAV-Cag-GFP HFD+CA=10* TGR5f/f-AAV-Cag-Cre-GFP HFD=10 *TGR5f/f-AAV-Cag-Cre-GFP HFD+CA=8*	Time (1): F(1.38,47.04)= 264.9 Genotype (2): F(1,34)=8.314 Diet (3): F(1,34)=24.65 1 x 2: F(20,680)=27.3 2 1 x 3: F(20,680)=98.5 0 2 x 3: F(1,34)=0.0001	Time (1): p<0.0001 Genotype (2): p=0.0068 Diet (3): p<0.0001 1 x 2: p<0.0001 1 x 3: p<0.0001 2 x 3: p=0.9938
4B	Body weight change (% HFD control)	Genotype	Unpaired t-test; two tailed	*TGR5^f/f* -AAV-Cag-GFP HFD+CA=10 *TGR5f/f-AAV-Cag-Cre-GFP HFD+CA=8*	t(16)=3.674	p=0.0021
4C	Fat mass change (% HFD control)	Genotype	Unpaired t-test; two tailed	*TGR5^f/f* -AAV-Cag-GFP HFD+CA=10 *TGR5f/f-AAV-Cag-Cre-GFP HFD+CA=8*	t(16)=4.939	p=0.0001
4D	Food intake (% HFD control)	Genotype	Unpaired t-test; two tailed	*TGR5^f/f* -AAV-Cag-GFP HFD+CA=10 *TGR5f/f-AAV-Cag-Cre-GFP HFD+CA=8*	t(16)=1.372	p=0.1889
4E	Feed efficiency (% HFD control)	Genotype	Unpaired t-test; two tailed	*TGR5^f/f* -AAV-Cag-GFP HFD+CA=10 *TGR5f/f-AAV-Cag-Cre-GFP HFD+CA=8*	t(16)=3.722	p=0.0019
S1B	Food intake	Time & Treatment	RM Two-way ANOVA	Vehicle=12 CCDC=15	Time: F(3,75)=489.6 Treatment: F(1,25)=5.836 Interaction: F(3,75)=6.873	Time: p<0.0001 Treatment: p=0.0233 Interaction: p=0.0004
S1C	Body weight change	Treatment	Unpaired t-test; two tailed	Vehicle=12 CCDC=15	t(25)=2.486	p=0.02
S1D	Food intake	Time & Treatment	RM Two-way ANOVA	Vehicle=6 CCDC=7	Time: F(24,264)=3.35 1 Treatment: F(1,11)=17.41 Interaction: F(24,264)=1.39 1	Time: p<0.0001 Treatment: p=0.0016 Interaction: p=0.1103
S1E	Glycemia AUC	Treatment	Unpaired t-test; two tailed	Vehicle=9 CCDC=16	t(23)=2.520	p=0.0191
S2A	Energy expenditure	Time, Treatment & Temperature	RM Three-way ANOVA	6 per group	Time (1): F(1,20)=160.2 Temperature (2): F(1,20)=112.3 Treatment (3): F(1,20)=4.987 1 x 2: F(1,20)=0.1730 1 x 3: F(1,20)=7.720 2 x 3: F(1,20)=0.2594	Time (1): p<0.0001 Temperature (2): p<0.0001 Treatment (3): p=0.0371 1 x 2: p=0.6819 1 x 3: p=0.0116 2 x 3: p=0.6161
S2B	RER	Time and treatment	RM Two-way ANOVA	6 per group	Time: F (1,10) = 1.906 Treatment: F (1,10) = 2.381 Interaction: F (1,10) = 0.003	Time: p=0.1975 Treatment: p=0.1538 Interaction: p=0.9510
S2C	Locomotor activity	Time and treatment	RM Two-way ANOVA	6 per group	Time: F (1,10) = 16.92 Treatment: F (1,10) = 0.2970	Time: p=0.0021 Treatment: p=0.5977

					Interaction: F (1,10) = 0.1597	Interaction: p=0.6979
S2D	Mean meal size	Time and treatment	RM Two-way ANOVA	6 per group	Time: F (1, 10) = 5.814 Treatment: F (1, 10) = 1.000 Interaction: F (1, 10) = 0.2326	Time: p=0.0366 Treatment: p=0.3409 Interaction: p=0.6400
S2E	Mean meal size	Time and treatment	RM Two-way ANOVA	6 per group	Time: F (1, 10) = 3.621 Treatment: F (1, 10) = 0.1497 Interaction: F (1, 10) = 0.04012	Time: p=0.0862 Treatment: p=0.7069 Interaction: p=0.8453
S2F	Plasma BA	Treatment	Mann Whitney *U* test; two tailed	Vehicle=8 CCDC=10	**Total BA** *U*:34 **CA** *U*:33.50 **DCA** *U*:38 **CDCA** (traces) no stat due to low N **UDCA** *U*:26 **LCA** (traces) no stat due to low N **αMCA** *U*:26 **βMCA** *U*:35 **ωMCA** *U*:27.50 **HDCA** *U*:33 **TCA** *U*: 29 **TDCA** *U*:38 **TCDCA** *U*:38 **TUDCA** *U*:37.50 **TLCA** N.D. **GCA** *U*:29 **TαMCA** *U*:31.50 **TβMCA** *U*:37 **TωMCA** *U*:36	**Total BA** p=0.6334 **CA** p=0.5687 **DCA** p=0.8767 **CDCA** no stat due to low N **UDCA** p=0.2177 **LCA** no stat due to low N **αMCA** p=0.3899 **βMCA** p=0.6805 **ωMCA** p=0.2845 **HDCA** p=0.5590 **TCA** p=0.3599 **TDCA** p=0.8968 **TCDCA** p=0.8797 **TUDCA** p=0.8463 **TLCA** N.D. **GCA** p=0.3188 **TαMCA** p=0.4738 **TβMCA** p=0.8100 **TωMCA** p=0.7618
S2G	Ratio	Treatment	Unpaired t-test or Mann Whitney *U* test; two tailed	4 per group	WAT: *U*=0 BAT: t(6)=4.501	WAT: p=0.0286 BAT: p=0.0041
S3C	DeltaCT	Genotype	Unpaired t-test or Mann Whitney U test; two tailed	*TGR5^f/f*-AAV-Cag-GFP=6 *TGR5f/f-AAV-Cag-Cre-GFP=8*	Hypothalamus: *U*=7 Cortex: t(12)=0.4814 Amygdala: t(12)=0.6634 VTA: t(12)=0.02542	Hypothal: p=0.0293 Cortex: p=06389 Amygdala: p=0.5196 VTA: p=0.9801
S3D	Food intake	Time & Genotype	RM Two-way ANOVA	*TGR5^f/f*-AAV-Cag-GFP=6 *TGR5f/f-AAV-Cag-Cre-GFP=8 C57BL/6J -AAV-Cag-Cre-GFP=7*	Time: F(13,234)=136.5 Treatment: F(2,18)=4.311 Interaction: F(26,234)=1.778	Time: p<0.0001 Treatment: p=0.0295 Interaction: p=0.0141
S3E	Food intake	Time & Genotype	RM Two-way ANOVA	*TGR5^f/f*-AAV-Cag-GFP=9 *TGR5f/f-AAV-Cag-Cre-GFP=10*	Time: F (12, 204) = 1.882 Treatment: F (1, 17) = 4.462 Interaction: F (12, 204) = 1.229	Time: p=0.0383 Treatment: p=0.0497 Interaction: p=0.2648
S4C	DeltaCT	Genotype	Unpaired t-test; two tailed	7 per group	t(12)=2.313	P=0.0392
S4D	Body weight	Time & Genotype	RM Two-way ANOVA	*TGR5^f/f*-AAV-GFAP-mCherry=7 *TGR5f/f-AAV-GFAP-Cre-mCherry=8*	Time: F(21,273)=448.7 Genotype: F(1,13)=0.0138 Interaction: F(21,273)=0.971	Time: p<0.0001 Genotype: p=0.9080 Interaction: p=0.4998
S4E	Fat mass	Genotype	Unpaired t-test; two tailed	*TGR5^f/f*-AAV-GFAP-mCherry=7 *TGR5f/f-AAV-GFAP-Cre-mCherry=8*	t(13)=0.4647	p=0.6499
S4F	Lean mass	Genotype	Unpaired t-test; two tailed	*TGR5^f/f*-AAV-GFAP-mCherry=7 *TGR5^f/f*-AAV-GFAP-Cre-mCherry=8	t(13)=0.7074	p=0.4918

S4G	Cumulative food intake	Genotype	Unpaired t-test; two tailed	*TGR5^{f/f}*-AAV-GFAP-mCherry=7 *TGR5f/f-AAV-GFAP-Cre-mCherry=8*	t(13)=0.0765	p=0.9401
S4H	Feed efficiency	Genotype	Unpaired t-test; two tailed	*TGR5^{f/f}*-AAV-GFAP-mCherry=7 *TGR5f/f-AAV-GFAP-Cre-mCherry=8*	t(13)=1.382	p=0.1903
S5A	Food intake	Time, Genotype & Diet	RM Three-way ANOVA	*TGR5^{f/f}*-AAV-Cag-GFP HFD=10 *TGR5f/f-AAV-Cag-GFP HFD+CA=10 TGR5f/f-AAV-Cag-Cre-GFP HFD=10 TGR5f/f-AAV-Cag-Cre-GFP HFD+CA=8*	Time (1): F(13,442)=31.31 Genotype (2): F(1,34)=13.88 Diet (3): F(1,34)=36.84 1 x 2: F(13,442)=1.245 1 x 3: F(13,442)=4.236 2 x 3: F(1,34)=0.2542	Time (1): p<0.0001 Genotype (2): p=0.0007 Diet (3): p<0.0001 1 x 2: p=0.2442 1 x 3: p<0.0001 2 x 3: p=0.617
S5B	Cumulative food intake	Diet & Genotype	Two-way ANOVA	*TGR5f/f-AAV-Cag-GFP HFD=10 TGR5f/f-AAV-Cag-GFP HFD+CA=10 TGR5f/f-AAV-Cag-Cre-GFP HFD=10 TGR5f/f-AAV-Cag-Cre-GFP HFD+CA=8*	Diet: F(1,34)=36.84 Genotype: F(1,34)=14.54 Interaction: F(1,34)=0.4579	Diet: p<0.0001 Genotype: p=0.0006 Interaction: p=0.5032
S5C	Body weight gain	Diet & Genotype	Two-way ANOVA	*TGR5f/f-AAV-Cag-GFP HFD=10 TGR5f/f-AAV-Cag-GFP HFD+CA=10 TGR5f/f-AAV-Cag-Cre-GFP HFD=10 TGR5f/f-AAV-Cag-Cre-GFP HFD+CA=8*	Diet: F(1,34)=164.0 Genotype: F(1,34)=24.91 Interaction: F(1,34)=0.3046	Diet: p<0.0001 Genotype: p<0.0001 Interaction: p=0.5846
S5D	Fat mass gain	Diet & Genotype	Two-way ANOVA	*TGR5f/f-AAV-Cag-GFP HFD=10 TGR5f/f-AAV-Cag-GFP HFD+CA=10 TGR5f/f-AAV-Cag-Cre-GFP HFD=10 TGR5f/f-AAV-Cag-Cre-GFP HFD+CA=8*	Diet: F (1, 34) = 105.3 Genotype: F (1, 34) = 37.68 Interaction: F (1, 34) = 0.01091	Diet: p<0.0001 Genotype: p<0.0001 Interaction: p=0.9174
S5E	Feed efficiency	Diet & Genotype	Two-way ANOVA	*TGR5f/f-AAV-Cag-GFP HFD=10 TGR5f/f-AAV-Cag-GFP HFD+CA=10 TGR5f/f-AAV-Cag-Cre-GFP HFD=10 TGR5f/f-AAV-Cag-Cre-GFP HFD+CA=8*	Diet: F(1,34)=261.5 Genotype: F(1,34)=37.47 Interaction: F(1,34)=0.7745	Diet: p<0.0001 Genotype: p<0.0001 Interaction: p=0.3850
S5F	Food intake	Diet	Mann Whitney *U* test; two tailed	5 per group	*U*=0	p=0.0079